The Canadian Mineralogist
Vol. 42, pp. 631-650 (2004)

Ru–Os–Ir–Pt AND Pt–Fe ALLOYS FROM THE EVANDER GOLDFIELD, WITWATERSRAND BASIN, SOUTH AFRICA: DETRITAL ORIGIN INFERRED FROM COMPOSITIONAL AND OSMIUM-ISOTOPE DATA

KRESHIMIR N. MALITCH[§]

Mineralogy and Petrology Group, Institute of Geological Sciences, University of Leoben, Peter Tunner Strasse 5, A–8700 Leoben, Austria and NATI Research JSC, Otechestvennaya 3–3a, St. Petersburg, 195030, Russia

ROLAND K.W. MERKLE[§]

Applied Mineralogy Group, Department of Geology, University of Pretoria, Pretoria 0002, South Africa

ABSTRACT

The compositionally diverse platinum-group minerals (PGM) from the Evander Goldfield, in the eastern part of the Witwatersrand Basin, South Africa, have been studied for the first time by a number of modern techniques. The characteristic feature of PGM from Evander is an extensive presence of Ru-rich alloys (*i.e.*, Ru–Os–Ir, Ru–Os–Ir–Pt, Ru–Ir–Pt, Ru–Pt), which prevail over osmium, iridium, rutheniridosmine, Pt–Fe, Pt–Ru–Fe and Pt–Ir–Os alloys and other PGM. The $^{187}Os/^{188}Os$ value, measured by N–TIMS in PGM that contain Os in the range 18–53 wt.% (*i.e.,* Pt–Ir–Os alloy, ruthenium, rutheniridosmine and osmium), varies from 0.0987 to 0.1068, revealing the lowest three $^{187}Os/^{188}Os$ values (0.0987–0.1024) reported so far in terrestrial PGM. The $^{187}Os/^{188}Os$ value measured by LA MC–ICP–MS in PGM with Os contents between 2 and 10 wt.% (Pt–Fe, Ru–Ir–Pt and Ru–Pt alloys) was found to range from 0.1053 to 0.1095. The model $^{187}Os/^{188}Os$ ages obtained for the main set of PGM (4104–3020 Ma, $n = 12$) imply that the PGM are detrital and were thus not deposited by later hydrothermal fluids. They also favor a scenario in which the majority of PGM were incorporated into the Witwatersrand basin by their release during weathering of ultramafic or mafic source-rocks.

Keywords: platinum-group minerals, electron-microprobe data, N–TIMS, LA MC–ICP–MS, osmium isotopes, model $^{187}Os/^{188}Os$ age, Evander Goldfield, Witwatersrand, South Africa.

SOMMAIRE

Nous avons étudié une diversité de minéraux du groupe du platine (MGP) provenant du champ aurifère de Evander, dans la partie orientale du bassin de Witwatersrand, en Afrique du Sud, pour la première fois par méthodes analytiques modernes. Ce qui distingue cette suite de MGP, c'est l'enrichissement en ruthénium dans les alliages (*i.e.*, Ru–Os–Ir, Ru–Os–Ir–Pt, Ru–Ir–Pt, Ru–Pt), qui prédominent sur l'omium, l'iridium, la rutheniridosmine, et les alliages Pt–Fe, Pt–Ru–Fe et Pt–Ir–Os, et autres MGP. La valeur du rapport $^{187}Os/^{188}Os$, telle que mesurée par N–TIMS dans les MGP qui contiennent entre 18 et 53% d'osmium (en poids), par exemple dans l'alliage Pt–Ir–Os, ruthénium, rutheniridosmine et osmium, varie de 0.0987 à 0.1068. Parmi ces résultats sont les trois valeurs les plus faibles du rapport $^{187}Os/^{188}Os$ (0.0987–0.1024) que l'on connaisse jusqu'à ce point dans les MGP terrestres. La valeur $^{187}Os/^{188}Os$ mesurée par LA MC–ICP–MS dans les MGP ayant des teneurs en osmium comprises entre 2 et 10% poids (par exemple, alliages Pt–Fe, Ru–Ir–Pt et Ru–Pt) varie entre 0.1053 et 0.1095. Les âges modèles $^{187}Os/^{188}Os$ obtenus pour la collection principale de MGP vont de 4104 à 3020 Ma ($n = 12$), ce qui implique que les MGP ont une origine détritique et non tardive et hydrothermale. Les résultats favorisent aussi un modèle évolutif selon lequel la majorité des MGP ont été concentrés dans le bassin de Witwatersrand une fois libérés par météorisation de roches ultramafiques ou mafiques.

(Traduit par la Rédaction)

Mots-clés: minéraux du groupe du platine, données à la microsonde électronique, N–TIMS, LA MC–ICP–MS, isotopes d'osmium, âge modèle $^{187}Os/^{188}Os$, champ aurifère de Evander, Witwatersrand, Afrique du Sud.

§ *E-mail addresses*: malitch@unileoben.ac.at, rmerkle@postino.up.ac.za

Introduction

The Late Archean paleoplacers of the Witwatersrand Basin, in South Africa, are not only unparalleled in their gold–uranium deposits, but have for many years also been the leading source of osmium. The osmium is present in the form of Os-rich platinum-group minerals (PGM), which are recovered as a by-product of gold-mining operations. The overall similarities in compositions of Os-rich concentrates throughout the basin have been documented (Cousins 1973). However, the Evander Goldfield, located at the eastern extremity of the Witwatersrand Basin (Fig. 1), differs from the other six goldfields (*i.e.,* East Rand, Central Rand, West Rand, Carletonville, Klerksdorp, and Welkom) in its higher *in situ* concentration of PGM and the lower than typical bulk (Os + Ir)/(Ru + Pt + Rh) and Ru/Pt values (Cousins 1973). Merkle & Franklyn (1999) and Malitch *et al.* (2000) showed that in Evander Goldfield, (1) the Os–Ir–Ru alloys have systematically higher Ru contents and (2) there are different modal proportions of chemically distinct PGM.

To demonstrate the high potential of Os isotopes measured in PGM, we expand our investigations to compositionally different PGM derived from the Kimberley Reef of the Evander Goldfield. Our combined osmium-isotope study [*i.e.,* negative thermal ionization mass-spectrometry (N–TIMS) and *in situ* laser ablation with multiple collector – inductively coupled plasma – mass spectrometry (LA MC–ICP–MS)] utilized the osmium-isotopic system of Ru–Os–Ir–Pt and Pt–Fe alloys from 13 selected nuggets, which had been characterized in advance by scanning electron microscopy (SEM) and electron-microprobe analysis (EMPA).

Our aim in this paper is to discuss osmium-isotopic compositions of various PGM at Evander in order to: (1) constrain the source of PGE in the Archean hinterland of the Witwatersrand basin on the basis of data for different PGM and their derivation from the mantle, (2) determine osmium-isotope signatures of this mantle source, (3) provide age constraints on the crystallization of the PGM, and (4) compare isotopic compositions of osmium in the PGM from different parts of the Witwatersrand Basin, specifying the possible bedrock source of PGM in the Witwatersrand paleoplacers.

Background Information

The first extensive osmium-isotope investigations of the Witwatersrand PGM were based on industrial concentrates from the Welkom Goldfield, which is located at the southern extremity of the basin (Hart & Kinloch

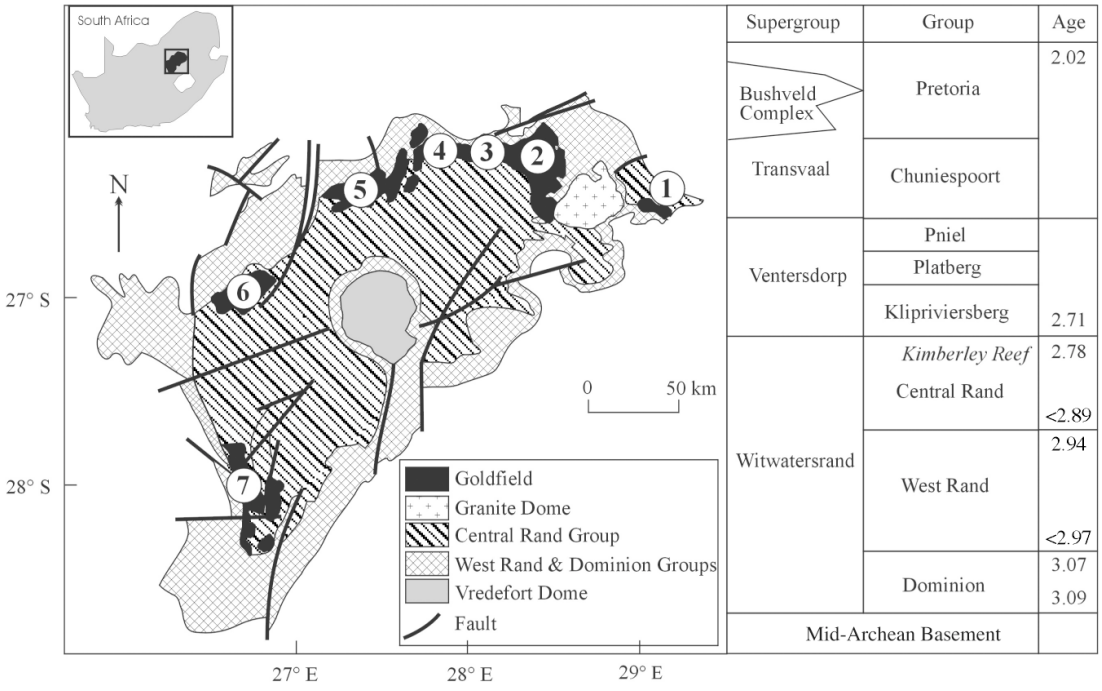

FIG. 1. Schematic map of the Witwatersrand Basin and location of the main goldfields: 1 Evander, 2 East Rand, 3 Central Rand, 4 West Rand, 5 Carletonville, 6 Klerksdorp, 7 Welkom. The stratigraphic column shows the position of the Kimberley Reef, from which the PGM were taken for our study.

1989). However, no mineralogical information on the PGM grains was provided. In order to avoid this incompleteness, a combination of compositional and osmium-isotope data for 12 grains of Os–Ir–Ru alloy (*i.e.,* osmium, iridium and ruthenium) from the Evander Goldfield has been presented by Malitch *et al*. (2000). For the major set of PGM (n = 10), independently of their chemical composition, two isotopically heterogeneous groups of PGM were established, with model $^{187}Os/^{188}Os$ ages of 3220 ± 70 and 3040 ± 40 Ma, respectively. These results indicated the high stability of the osmium-isotope system at the single-crystal scale; it had not been affected by later thermal events.

Recent developments in osmium-isotope measurements of Os-rich alloys and sulfides by N–TIMS (Creaser *et al*. 1991, Kostoyanov & Pushkaryov 1998, Kostoyanov *et al*. 2000) and by LA MC–ICP–MS (Hirata *et al*. 1998, Junk 2001, Malitch *et al*. 2003a) now make it possible to obtain extensive quantitative data both for Os-rich minerals and PGM with Os contents as low as a few wt% Os.

The presence of Os-rich minerals in different layers of the Witwatersrand Basin implies their introduction into the basin over a long time-space from a considerable number and variety of ultramafic and mafic rocks. This variability may be reflected in the isotopic composition of osmium in individual PGM grains and requires careful evaluation of the relationships of mineral compositions, textures, and osmium isotopes. Therefore, to ultimately characterize the PGM for which N–TIMS and LA MC–ICP–MS analyses have been done, the composition of PGM in selected nuggets also is presented, along with their morphology and internal texture.

Geological Setting and Sample Location

The Witwatersrand Basin is an erosional remnant of a much larger basin, formed over a long period of time (bracketed by zircon ages of 2970–2714 Ma: Robb & Meyer 1995) in the central and southern parts of the Kaapvaal Craton. In the interior of the Witwatersrand trough, three groups of sediments have been identified: Dominion Group, West Rand Group, and Central Rand Group (Fig. 1). The Witwatersrand Basin extends to the northeast for 300 km, and its width is 100 km. It consists of a very thick (>7 km) succession of quartzites, slates, and conglomerates mainly, that have a distinctive rhythmic structure (Du Toit 1954). Conglomerates make up less than 0.2% of the total thickness, forming 16 separate horizons (reefs) bearing gold and uranium accompanied by PGM, pyrite and a large suite of other heavy minerals. The main resources of gold are associated with conglomerates of the Central Rand Group. More detailed geological characteristics of the Witwatersrand Basin, along with aspects of the structure, composition and origin of productive conglomerates, are given, among others, by Young (1907), Du Toit (1954), Robb & Meyer (1990, 1995), Pretorius (1991), Minter *et al*. (1993), Phillips & Law (1994, 2000), Stevens *et al*. (1997), and Frimmel *et al*. (1999).

The average concentrations of PGE *in situ* are not precisely defined. However, the reported information on production along with estimated efficiency of extraction, imply average *in situ* concentrations of 3.5 wt-ppb ΣPGE (Cousins 1973), or a range of >100 to 4 wt-ppb (Reimer 1979) for various ore-bearing horizons. The grains of PGM described *in situ* in the Witwatersrand rocks or in production concentrates are invariably small, typical sizes being in the range from ~70 μm (Feather & Koen 1975, Oberthür 1983) to ~120 μm (Young 1907).

The PGM nuggets (*i.e.,* whole particles, which may consist of one to five distinct PGM) in this study were derived from a production concentrate from the Kimberley Conglomerate Formation (Kimberley Reef) of the Evander Goldfield. This reef is situated in the upper part of the Central Rand Group (Turffontein Subgroup of the Central Rand Group, Fig. 1) [South African Committee for Stratigraphy (SACS) 1980, Tweedie 1986, Tainton 1994], which appears to have a maximum age of ~2940 Ma. The time interval of deposition of the Central Rand Group sediments did not exceed 230 Ma and is constrained by the overlying igneous rocks of the Ventersdorp Supergroup (~2710 Ma: Armstrong *et al*. 1991). More detailed information on the geology of the Evander Goldfield has recently been summarized by Poujol *et al*. (1999).

The main Witwatersrand Basin to the west of Evander received its detrital material from source areas to the north, but there are strong indications that the source area for the Evander goldfield was located to the south or southwest (Cousins 1973, Pretorius 1981, Tweedie 1986, Minter & Leon 1991).

Analytical Techniques

The investigation was carried out in four main steps. First, the morphology of PGM grains represented by individual crystals and polymineralic aggregates was documented by SEM. The grains were then mounted and polished, described and analyzed by electron-microprobe analysis at Mechanobr–Analyt JSC, St. Petersburg, Russia (Camscan–4 with a Link–10 000 energy-dispersion spectrometer and a Microspec wavelength-dispersion spectrometer). Subsequently, chemical analyses of the PGM were carried out on an ARL–SEMQ electron microprobe equipped with four wavelength-dispersion spectrometers (WDS) and with a LINK energy-dispersion analyzer (EDS) at the Department of Mineralogy and Petrology, Institute of Geological Sciences, University of Leoben, Austria. Quantitative WDS analyses were performed at an accelerating voltage of 25 kV and a sample current of 20 nA, with a beam diameter of about 1 μm. The following X-ray lines and standards were used: Ru$L\alpha$, Rh$L\alpha$, Pd$L\beta$, Os$M\alpha$, Re$L\alpha$, Ir$L\alpha$, Pt$L\alpha$, Ni$K\alpha$, Co$K\alpha$ (all

native element standards); Fe$K\alpha$, Cu$K\alpha$, S$K\alpha$ (chalcopyrite, $CuFeS_2$); Te$L\alpha$ (kotulskite, PdTe), As$L\alpha$ (sperrylite, $PtAs_2$), and Sb$L\alpha$ (stibiopalladinite, $Pd_{5+x}Sb_{2-x}$). Corrections were performed for interferences involving Ru–Rh, Ru–Pd and Ir–Cu. A total of 256 quantitative analyses of PGM from 86 nuggets were made.

After the round of microprobe analyses, nine Os-rich PGM grains, with an Os content in the range of 18–53 wt.%, were removed from the resin for isotopic analysis. The osmium-isotope composition was determined on the individual PGM grains by N–TIMS using a modified MI–1320 instrument (Kostoyanov & Pushkaryov 1998, Kostoyanov *et al.* 2000) at the Department of Isotope Geology, All-Russia Geological Research Institute (VSEGEI), St. Petersburg, Russia. The precision of the osmium-isotope determinations, based on the reproducibility of isotope ratios in series of parallel runs, was found to be 0.3%. Concentrations of the osmium isotopes were determined by one-tape detection of negative OsO_3^- ions formed on the cathode surface at temperatures of 700–1400°C (Kostoyanov & Pushkaryov 1998). The method allows the analysis of individual PGM grains weighing as little as 10^{-7}g and containing more than 10 wt.% of osmium. The amount obtained from single grains of PGM was sufficient to maintain the signal of one of the most abundant isotopes of Os (^{190}Os) at 10^{-13}–10^{-14} ångström (Å) for several hours. Measured ratios of isotopes were normalized by taking into account both isobar and mass-fractionation effects. The mass-fractionation effect was considered to be exponentially related to the mass of the detected ion. During the measurements of the laboratory standard, OsO_2, no systematic errors were found. The ^{190}Os/^{188}Os value of independent runs of laboratory standard samples (1.9837 ± 0.0004, Kostoyanov *et al.* 2000) was within the range of random errors for the ^{190}Os/^{188}Os value of the DTM osmium standard measured with a MAT–262 (1.98378 ± 0.00002, Tuttas 1992). Further details on the method and analytical precisions are given in Kostoyanov *et al.* (2000) and Malitch *et al.* (2000).

Finally, three PGM grains with a lower Os content (*i.e.,* 2–10 wt.% Os) were investigated by LA MC–ICP–MS using a Microprobe II LA device (Thermo Elemental, Nd:YAG laser, 266 nm wavelength, up to 4 mJ per shot, 3 ns pulse width) and an AXIOM MC–ICP–MS (Thermo Elemental) at the Institute of Archaeometry, Technical University of Mining and Metallurgy, Freiberg, Germany. The ICP–MS was tuned using an desolvating nebulizer (MCN 6000, CETAC), a solution of 33 μg/L Re, 330 μg/L Os, and 330 μg/L Ir in 2% nitric acid, a nebulizer flow of 0.8 L/min Ar, and a radio frequency (RF) forward power of 1330 W. Helium was used as an ablation-chamber gas, with a flow of 85 mL/min in a chamber 2.5 cm in diameter that has a minimized dead volume. The air capacitor of the ICP–MS was optimized to obtain a RF reflected power of 12 to 18 W with this addition of He to the plasma gas. The Re and the W corrections were checked with a combined LA of a sample of the ferberite–hübnerite series, and the aerosol generated by the desolvating nebulizer, as described by Junk (2001).

Laser-ablation spots of 5 to 25 μm were used with a scan field adapted to the size of each sampling area, a laser-shot frequency of 20 Hz, and an energy output of up to 0.5 mJ. The aerosols generated by LA were transported by a gas stream to the MC–ICP–MS (Thermo-Elemental Axiom, multicollector version with nine Faraday cup detectors, resolution $m/\Delta m$ of 400). Nine signals were measured simultaneously, at m/z 183 (W), 184 (W + Os), 185 (Re), 186 (W + Os), 187 (Re + Os), 188 (Os), 189 (Os), 191 (Ir) and 193 (Ir). The mass bias was corrected using an exponential fractionation law and the ^{188}Os/^{189}Os value. Isobaric interferences were very rarely encountered and were thus corrected using the natural abundances of Re and W. Molecular interferences and problems connected with the abundance sensitivity were tested by using the ^{191}Ir/^{193}Ir ratio as a second-possibility mass-bias correction, as described by Junk (2001). For the reported values, no significant contribution of these possible sources of error was detected. The natural abundances used for the calculations were published as best experimental values by Rosman & Taylor (1998). The isotope ratios are reported with experimental uncertainties, taking into account the contributions of the Faraday cup efficiencies, the normalization value for mass-bias corrections using ^{188}Os/^{189}Os (Rosman & Taylor 1998), interference corrections, the noise associated with the signal, and the within-run standard deviations. A more detailed description of the method is given by Junk (2001) and Malitch *et al.* (2003a).

PGE Mineralogy

We found a high diversity of PGE alloys among 86 PGM nuggets studied (Table 1, Fig. 2). According to the nomenclature of Harris & Cabri (1991), alloys of ruthenium (54.5%) prevail over osmium (21.5%), iridium (8.5%) and Pt–Fe alloy (7%), in contrast to earlier reported mineral-chemical characteristics of the PGE mineralization from other parts of the Witwatersrand Basin (Cousins 1973, Feather 1976). Other alloys identified are unnamed alloys of Pt–Ru–Fe (3.5%), Pt–Ir–Os (2.5%) and rutheniridosmine (2.5%). The diversity of Ru-rich alloys, some of which represent uncommon solid-solution series in the system Ru–Os–Ir–Pt–Fe (Table 1, Fig. 2), is noteworthy. Many of the PGM nuggets have a characteristic internal structure consisting of a core and a polymineralic rim (Figs. 3, 4), previously described by Feather (1976). Unusual unnamed alloys of the system Ru–Os–Ir–Pt–Fe (Fig. 2) have been determined to be present both as monomineralic and polymineralic grains. Polyphase aggregates commonly

contain a core formed of Ru–Os–Ir–Pt, Ru–Os–Ir or Pt–Fe alloy, rimmed by sperrylite $PtAs_2$ (46 cases). In the polymineralic grains, in addition to various minerals of the system Ru–Os–Ir–Pt–Fe and sperrylite, Ru–Os sulfides (laurite and erlichmanite), an unnamed Ru–Ir sulfide, cooperite, PGE sulfarsenides (minerals of the irarsite – platarsite – hollingworthite series, ruarsite and unnamed Ru–Pt–Ir sulfarsenide), sudburyite and polkanovite have been identified. Further details of the considerable variety of PGE alloys and associated PGM will be presented elsewhere.

Chemical Composition of Selected PGM Nuggets

A list of all the PGM found in the nuggets selected is presented in Table 2. The compositional features of PGM nuggets, along with morphology and details of their internal texture, are illustrated in Figures 2 to 5. The chemical compositions of single PGM and polyphase PGM nuggets, which were measured by N–TIMS and LA MC–ICP–MS, are given in Tables 3 and 4. Grain shapes range from well rounded to irregular (Figs. 3, 4), with sizes of PGM nuggets between 68 and 158 μm.

Osmium was documented in three monophase and two polyphase PGM nuggets (Table 2). In polyphase nuggets, osmium forms either a core rimmed by sperrylite (grain W1 3–13, Fig. 3a, b) or it rims a complex assemblage of PGM dominated by Pt–Ir–Os and Pt–Fe alloys, with subordinate laurite and cooperite (grain W3 39, Fig. 3f). Chemically, according to the abundance of the iridium group of the platinum-group elements (IPGE), *i.e.*, iridium, osmium and ruthenium, osmium can be subdivided into three main varieties (Figs. 3, 5A), (1) Os–Ru–Ir alloy with a corresponding formula $Os_{0.34–0.40}Ru_{0.29–0.31}Ir_{0.23–0.26}Pt_{0.07–0.08}$ (grains W1 3–13 and W1 2–2, Table 3, anal. 1 and 8, respectively), (2) Os–Ir–Ru alloy ($Os_{0.35}Ir_{0.34}Ru_{0.27}Rh_{0.02}Pt_{0.01}Fe_{0.01}$) (grain W3 37, Table 3, anal. 6), and (3) iridian osmium (grains W3 28 and W3 60, Table 3, anal. 3 and 10, respectively, and grain W3 39, Table 4, anal. 19) that contains moderate concentrations of Ru (3.59–4.67 wt.%, 6.64–8.33 at.%), Fe (up to 1.28 wt.%, 4.09 at.%), and low Ni (up to 0.36 wt.%, 1.09 at.%) and Pt (up to 0.45 wt.%, 0.43 at.%). The composition of the Os-rich alloys displays a large variation in terms of Ru# [= $100*Ru_{at.\%}/(Ru + Os)_{at.\%}$]. In iridian osmium, the Ru# varies from 10 to 14, whereas in Os–Ru–Ir and Os–Ru–Ir alloys, it increases to 42–48 (Table 3, anal. 1, 3, 6, 8 and 10; Table 4, anal. 6).

Ruthenium was observed in two single-phase and three polyphase PGM nuggets (Table 2). In two polyphase grains, it is rimmed by sperrylite (grains W1 2–18, Fig. 4a, c; W1 3–14, Fig. 4b, d, f), whereas in the third assemblage, ruthenium and sperrylite are divided by an intervening layer of hollingworthite RhAsS, similar to the case described as Figure 3 by Feather (1976). Chemically, ruthenium is represented by several varieties of minerals: (1) Ru–Os–Ir(±Pt) and (2) Ru–Ir–Pt and

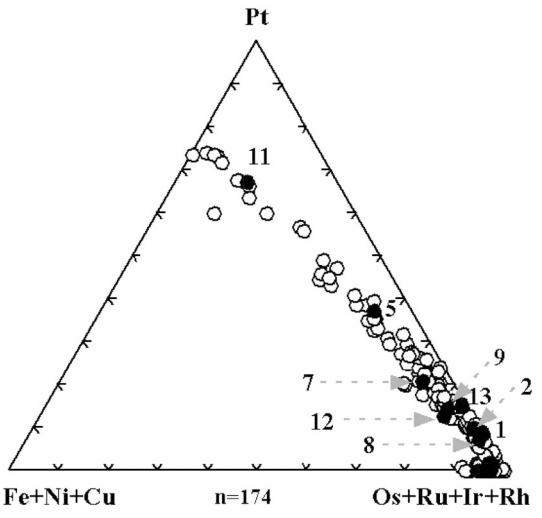

FIG. 2. Composition of Ru–Os–Ir–Pt and Pt–Fe alloys from the Evander goldfield in the diagram (at.%) Pt – Fe + Ni + Cu – Ru + Os + Ir + Rh. Numbers 1, 2, 5, 7–9 and 11–13 correspond to the same numbers in Tables 3 and 5. Black circles indicate PGM grains studied by N–TIMS and LA MC–ICP–MS.

TABLE 1. ABUNDANCES OF PGE ALLOYS (%) IN THE EVANDER GOLDFIELD

PGE alloys	#	%	PGE alloys	#	%
Ruthenium (Ru,Os,Ir,Pt)	12		Iridium (Ir,Os)	4	
Ruthenium (Ru,Pt,Os,Ir)	8		Iridium (Ir,Ru,Os)	2	
Ruthenium (Ru,Ir,Os,Pt)	7		Iridium (Ir,Ru,Os,Pt)	2	
Ruthenium (Ru,Pt,Ir,Os)	6		Iridium (Ir,Pt,Os,Ru)	2	
Ruthenium (Ru,Os,Ir), (Ru,Os)	6		*Total iridium grains*	*10*	*8.5*
Ruthenium (Ru,Pt)	5				
Ruthenium (Ru,Pt,Ir)	5		*Total Pt–Fe grains*	*8*	*7*
Ruthenium (Ru,Ir,Pt)	5				
Ruthenium (Ru,Ir,Os)	3		(Pt,Ru,Fe)	3	
Ruthenium (Ru,Ir)	2		(Pt,Ru,Ir,Fe)	1	
Ruthenium (Ru,Ir,Pt,Os)	1		*Total*	*4*	*3.5*
Ruthenium (Ru,Os,Pt,Ir)	1				
Ruthenium (Ru,Pt,Ir,Fe)	1		(Pt,Ir,Os)	2	
Ruthenium (Ru,Ir,Rh)	1		(Pt,Ir,Os,Fe)	1	
Total ruthenium grains	*63*	*54.5*	*Total*	*3*	*2.5*
Osmium (Os, Ir)	12		Rutheniridosmine (Ir,Os,Ru,Pt)	2	
Osmium (Os,Ir, Ru)	5		Rutheniridosmine (Ir,Os,Pt,Ru)	1	
Osmium (Os,Ru,Ir)	5		*Total*	*3*	*2.5*
Osmium (Os,Ru,Ir,Pt)	2				
Osmium (Os)	1				
Total osmium grains	*25*	*21.5*			

Number of grains of PGE alloy counted, also expressed as a percentage of the total, 116 grains in 86 nuggets.

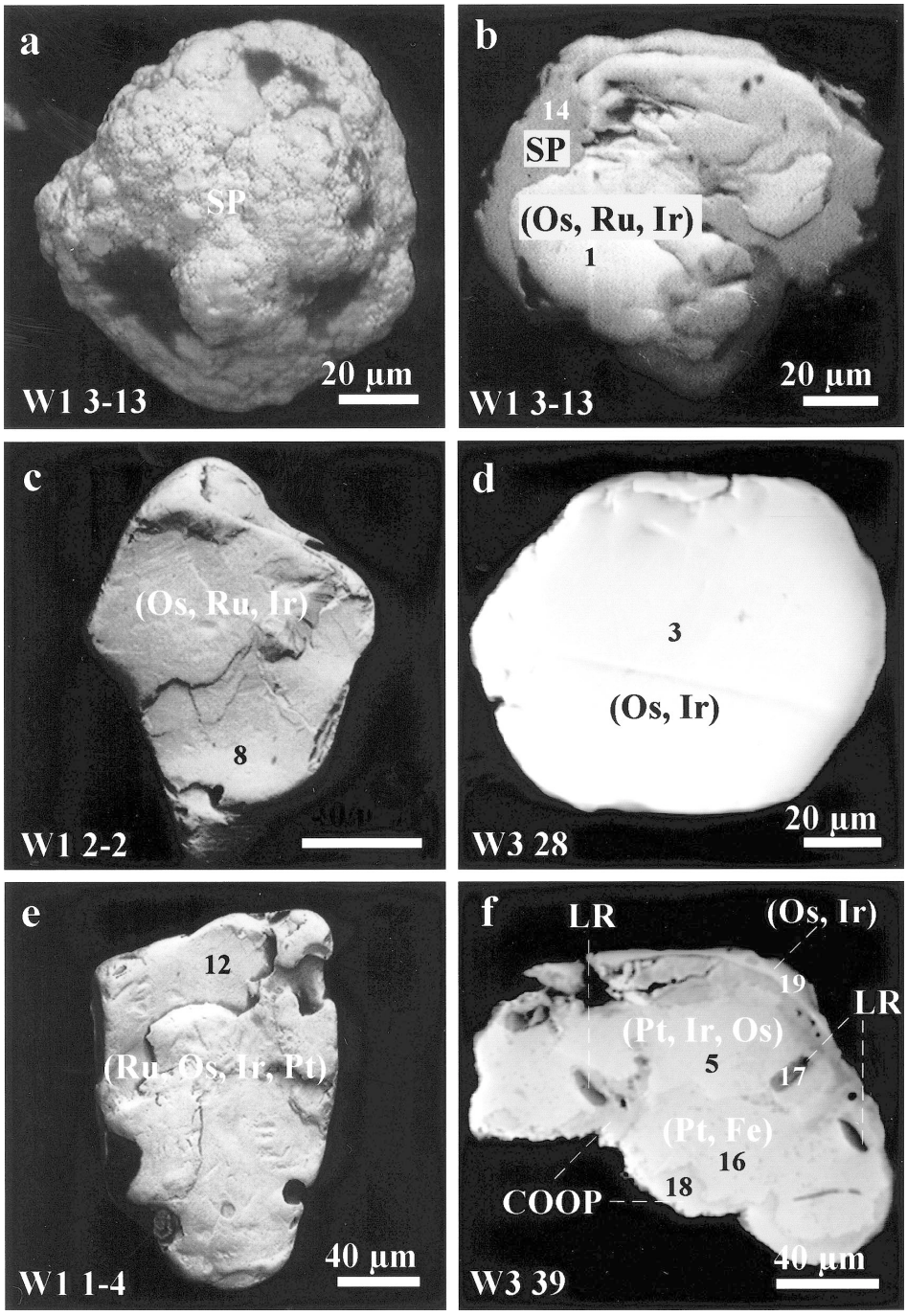

FIG. 3. Scanning electron microscope (SEM: a, c, e) and back-scattered electron (BSE: b, d, f) images of single and polyphase PGM grains from Evander, showing morphology (a, c, e) and internal texture (b, d, f) of PGM assemblages. (Os, Ru, Ir), (Os, Ir): osmium, (Ru, Os, Ir, Pt): ruthenium, (Pt, Ir, Os):Pt–Ir–Os alloy, (Pt, Fe): Pt–Fe alloy, LR: laurite, COOP: cooperite, SP: sperrylite; numbers 1, 3, 5, 8, 12, 14, 16–19 denote areas of electron-microprobe analyses corresponding to the same numbers in Tables 3 and 4.

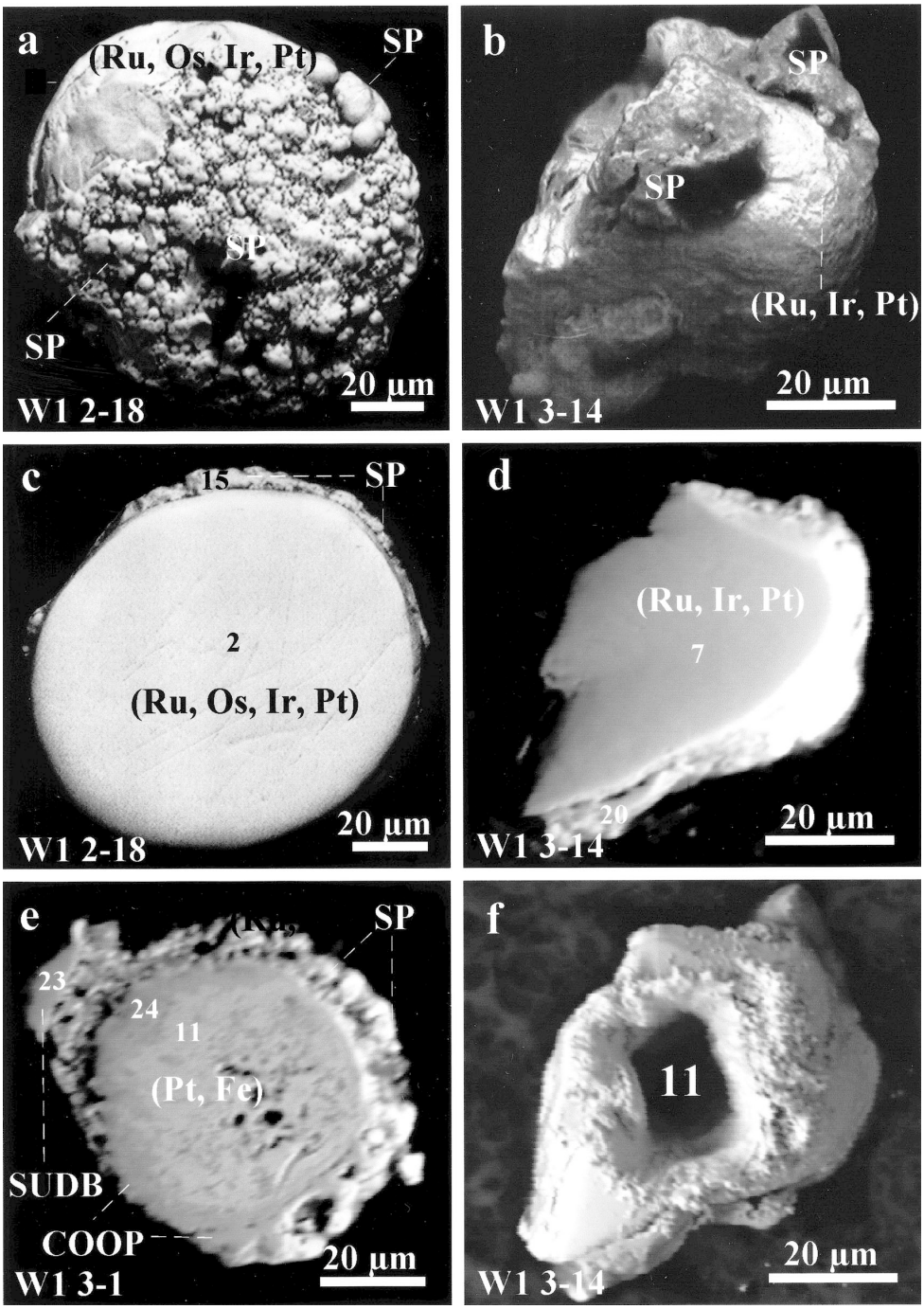

FIG. 4. Morphology (a, b) and internal texture (c–f) of polyphase PGM grains from Evander before (a–e) and after (f) laser ablation MC–ICP–MS. (Ru, Os, It, Pt): ruthenium, (Ru, Ir, Pt): Ru–Ir–Pt alloy, (Pt, Fe): Pt–Fe alloy, SP: sperrylite, COOP: cooperite, SUDB: sudburyite. Numbers 2, 7, 11, 15, 20, 22–24 denote areas of electron-microprobe analyses corresponding to the same numbers in Tables 3 and 4. Number 11 in black hole (Fig. 4f) indicates the area of laser ablation MC–ICP–MS analysis, which corresponds to the same number in Table 5. SEM (a, b) and BSE (c–f) images.

TABLE 2. LIST OF PGM OBSERVED IN SELECTED Ru–Os–Ir–Pt AND Pt–Fe NUGGETS FROM THE EVANDER GOLDFIELD, WITWATERSRAND, ACCORDING TO MICRO-ANALYTICAL DATA

Number	1	2	3	4	5	6	7	8	9	10	11	12	13
Sample	W1 3–13	W1 2–18	W3 28	W3 36	W3 39	W3 37	W1 3–14	W1 2–2	W3 33	W3 60	W1 3–1	W1 1–4	W1 1–7
Figure	3a, b	4a, c	3d		3f		4b, d, f	3c			4e	3e	
Osmium (Os,Ru,Ir)	●							●					
Osmium (Os,Ir)			●							●			
Osmium (Os,Ir,Ru)						●							
Ruthenium (Ru,Os,Ir), (Ru,Os,Ir,Pt)		●		●								●	
Ruthenium (Ru,Ir,Pt), (Ru,Pt)							●						●
Rutheniridosmine (Ir,Os,Pt,Ru)									●				
Pt–Ir–Os alloy					●								
Pt–Fe alloy					●						●		
Sudburyite PdSb											•		
Sperrylite $PtAs_2$	•	•					•		•		•		•
Laurite RuS_2					•								
Cooperite PtS					•						•		
Hollingworthite RhAsS													•
Quartz SiO_2													•

●: major PGM, •: minor PGM.

TABLE 3. REPRESENTATIVE COMPOSITIONS OF PGE ALLOYS FROM THE EVANDER GOLDFIELD

No.	1	2	3	4	5	6	7	8	9	10	11	12	13
Fe wt.%	0.00	0.49	0.61	0.64	2.39	0.50	2.21	0.31	1.31	1.28	5.84	2.06	0.46
Ni	0.00	0.00	0.29	0.17	0.10	0.15	0.00	0.31	0.00	0.36	0.00	0.23	0.00
Cu	0.00	0.00	0.00	0.00	0.00	0.00	0.00	0.00	0.00	0.00	0.27	0.00	0.00
Ru	17.30	21.69	4.67	26.61	3.54	16.93	25.41	19.33	7.28	4.56	2.15	29.99	54.75
Rh	0.00	0.00	0.00	0.50	1.05	0.94	0.00	0.00	0.00	0.00	1.92	0.00	0.00
Pd	0.00	0.00	0.00	0.00	0.26	0.00	0.00	0.00	0.00	0.00	1.13	0.00	0.00
Os	45.38	38.92	52.63	46.98	17.81	40.26	8.95	39.73	35.62	72.56	2.02	24.93	10.27
Ir	26.11	25.90	41.54	21.66	32.49	39.68	35.94	30.28	38.91	20.12	7.06	24.91	11.74
Pt	10.03	12.25	0.00	2.58	40.76	1.65	27.08	8.46	16.05	0.00	79.07	16.98	22.72
Total	98.82	99.25	99.74	99.14	98.40	100.11	99.59	98.42	99.17	98.88	99.46	99.10	99.94
Fe at.%	0.00	1.40	1.97	1.75	7.59	1.46	5.96	0.91	4.13	4.09	17.09	5.38	1.05
Ni	0.00	0.00	0.89	0.44	0.30	0.42	0.00	0.86	0.00	1.09	0.00	0.57	0.00
Cu	0.00	0.00	0.00	0.00	0.00	0.00	0.00	0.00	0.00	0.00	0.69	0.00	0.00
Ru	28.67	34.31	8.33	40.17	6.21	27.25	37.87	31.26	12.69	8.05	3.48	43.30	69.32
Rh	0.00	0.00	0.00	0.74	1.80	1.48	0.00	0.00	0.00	0.00	3.05	0.00	0.00
Pd	0.00	0.00	0.00	0.00	0.43	0.00	0.00	0.00	0.00	0.00	1.74	0.00	0.00
Os	39.96	32.71	49.87	37.69	16.61	34.44	7.09	34.14	33.00	68.08	1.74	19.13	6.91
Ir	22.75	21.54	38.95	17.19	29.98	33.58	28.17	25.75	35.67	18.68	6.00	18.91	7.82
Pt	8.61	10.04	0.00	2.02	37.06	1.38	20.91	7.09	14.50	0.00	66.22	12.70	14.90
Pt/Os	0.22	0.31	0.00	0.05	2.23	0.04	2.95	0.21	0.44	0.00	38.16	0.66	2.16
Ru number	42	51	14	52	27	44	84	48	28	11		69	91

Numbers 1–13 refer to points on Figures 2–6 showing where the electron-microprobe analyses were made. Samples: 1: W1 3-13, osmium, Figures 3a, b; 2: W1 2-18, ruthenium, Figures 4a, c; 3: W3 28, osmium, Figure 3d; 4: W3 36, ruthenium; 5: W3 39, Pt–Ir–Os alloy, Figure 3f; 6: W3 37, osmium; 7: W1 3-14, Ru–Ir–Pt alloy, Figures 4b, d, f; 8: W1 2-2, osmium, Figure 3c; 9: W3 33, rutheniridosmine; 10: W3 60, osmium; 11: W1 3-1, Pt-Fe alloy, Figure 4e; 12: W1 1-4, ruthenium, Figure 3e; 13: W1 1-7, Ru–Pt alloy. Ru number: 100*Ru/(Ru + Os), the concentrations being expressed in at.%. The concentration of Re is below the detection limit of electron-microprobe analysis.

TABLE 4. REPRESENTATIVE COMPOSITIONS OF PGM FROM SELECTED NUGGETS AT EVANDER

No.	14	15	16	17	18	19	20	21	22	23	24
S wt.%	1.95	1.00	0.00	35.88	15.18	0.00	1.00	1.74	1.68	0.00	17.28
As	37.69	40.27	0.00	0.00	0.00	0.00	46.23	42.55	41.43	0.00	2.40
Sb	1.24	1.29	n.d.	n.d.	n.d.	n.d	1.10	n.d.	1.68	52.77	0.00
Te	1.04	0.70	n.d	n.d.	n.d.	n.d	0.00	n.d.	0.00	0.00	0.00
Co	1.29	0.42	n.d	n.d.	n.d.	n.d	2.04	n.d.	0.86	0.00	0.00
Fe	0.58	0.29	6.09	0.00	0.11	0.00	1.00	0.25	0.00	0.00	0.67
Ni	0.33	0.34	0.14	0.00	0.19	0.00	1.25	0.14	0.63	0.00	0.10
Cu	0.00	0.00	0.97	0.00	0.00	0.00	0.00	0.00	0.00	0.00	0.00
Ru	0.00	0.00	0.64	48.61	0.00	3.59	0.00	0.00	0.00	0.00	6.88
Rh	1.74	0.00	0.81	0.00	0.36	0.00	0.70	1.25	0.00	0.00	3.30
Pd	0.00	0.00	0.64	0.00	0.38	0.00	0.00	0.17	0.00	46.26	0.42
Os	1.09	0.00	0.68	8.83	0.10	59.68	0.00	0.00	0.00	0.00	0.70
Ir	2.67	0.00	4.87	4.85	0.00	35.22	0.00	0.58	0.00	0.00	3.49
Pt	50.32	54.59	83.53	0.00	84.01	0.45	46.71	52.90	53.54	0.00	63.83
Total	99.94	98.90	98.37	98.17	100.33	98.94	100.03	99.58	99.82	99.03	99.07
S at.%	6.65	3.53	0.00	66.94	51.64	0.00	3.19	5.92	5.70	0.00	51.93
As	55.01	60.89	0.00	0.00	0.00	0.00	63.14	61.94	60.17	0.00	3.09
Sb	1.11	1.20	-	-	-	-	0.92	-	1.50	49.92	0.00
Te	0.89	0.62	-	-	-	-	0.00	-	0.00	0.00	0.00
Co	2.39	0.81	-	-	-	-	3.54	-	1.59	0.00	0.00
Fe	1.14	0.59	18.05	0.00	0.21	0.00	1.83	0.49	0.00	0.00	1.16
Ni	0.61	0.66	0.39	0.00	0.35	0.00	2.18	0.26	1.17	0.00	0.16
Cu	0.00	0.00	2.53	0.00	0.00	0.00	0.00	0.00	0.00	0.00	0.00
Ru	0.00	0.00	1.05	28.77	0.00	6.64	0.00	0.00	0.00	0.00	6.56
Rh	1.85	0.00	1.31	0.00	0.38	0.00	0.70	1.32	0.00	0.00	3.09
Pd	0.00	0.00	1.00	0.00	0.39	0.00	0.00	0.17	0.00	50.08	0.38
Os	0.63	0.00	0.59	2.78	0.06	58.67	0.00	0.00	0.00	0.00	0.35
Ir	1.52	0.00	4.19	1.51	0.00	34.26	0.00	0.33	0.00	0.00	1.75
Pt	28.20	31.70	70.89	0.00	46.97	0.43	24.50	29.57	29.87	0.00	31.53

Numbers 14–24 refer to points on Figures 3 and 4 showing where the electron-microprobe analyses were made. Samples: 14: W1 3-13, sperrylite, Figures 3a, b; 15: W1 2-18, sperrylite, Figures 4a, c; 16: W3 39, Pt–Fe alloy, Figure 3f; 17: W3 39, laurite, Figure 3f; 18: W3 39, cooperite, Figure 3f; 19: W3 39, osmium, Figure 3f; 20: W1 3-14, sperrylite, Figures 4b, d, f; 21: W3 33, sperrylite; 22: W1 3-1, sperrylite, Figure 4e; 23: W1 3-1, sudburyite, Figure 4e; 24: W1 3-1, cooperite, Figure 4e. n.d.: not determined.

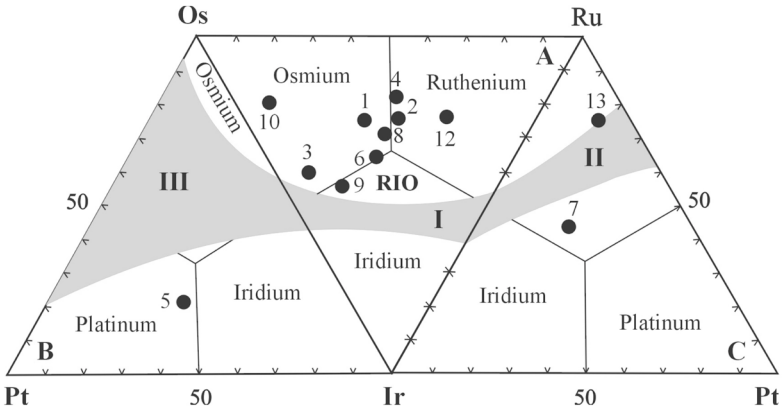

FIG. 5. Composition of Ru–Os–Ir, Pt–Os–Ir and Ru–Pt–Ir alloys from the Evander Goldfield in terms of the diagrams (at.%) Ru–Os–Ir (A), Pt–Os–Ir (B) and Pt–Ru–Ir (C), respectively. RIO: rutheniridosmine, fields I, II and III denote a miscibility gap. Numbers 1–10, 12 and 13 correspond to the same numbers in Table 3.

Ru–Pt alloys, which belong to different solid-solution series in the system Ru–Os–Ir(±Pt) and Ru–Ir–Pt (Table 3, anal. 2, 4, 7, 12, 13; Figs. 5A, C). In the system Ru–Os–Ir(±Pt), ruthenium alloys have a compositional range between ($Ru_{0.34–0.40}Os_{0.33–0.38}Ir_{0.17–0.22}Pt_{0.02–0.10}Fe_{0.01–0.02}$) and ($Ru_{0.43}Os_{0.20}Ir_{0.19}Pt_{0.13}Fe_{0.05}$); in the system Ru–Ir–Pt, Ru-rich minerals have an even broader range of compositions, from ($Ru_{0.38}Ir_{0.28}Pt_{0.21}Os_{0.07}Fe_{0.06}$) to ($Ru_{0.69}Pt_{0.15}Ir_{0.08}Os_{0.07}Fe_{0.01}$). Consequently, Ru-rich alloys are characterized by Ru# in the range of 51–69 and 84–91 (Table 3, anal. 2, 4, 7, 12, 13; Figs. 5A, C).

Rutheniridosmine was identified in association with sperrylite in grain W3 33 (Table 2). It contains significant concentrations of Pt (16.05 wt.%, 14.50 at.%) and Fe (1.31 wt.%, 4.13 at.%), which likely substitute for Ir, corresponding to the formula ($Ir_{0.36}Os_{0.33}Pt_{0.14}Ru_{0.13}Fe_{0.04}$) (Table 3, anal. 9; Fig. 5A).

Pt–Ir–Os alloy was found in the polyphase assemblage of grain W3 39 (Table 2, Fig. 3f), associated with Pt–Fe alloy, Os–Ir alloy, laurite and cooperite. It corresponds to the formula ($Pt_{0.38}Ir_{0.30}Os_{0.17}Fe_{0.07}Ru_{0.06}Rh_{0.02}$) (Table 3, anal. 5; Fig. 5B) and matches perfectly the compositional trend of complex alloys in the system Pt – Fe + Ni + Cu – Os + Ir + Ru + Rh (Fig. 2) that was first proposed by Feather (1976).

Pt–Fe alloy was identified in two polyphase grains (Table 2). In grain W3 39, it occurs with Pt–Os–Ir and Os–Ir alloys, laurite and cooperite (Fig. 3f), whereas in grain W1 3–1, Pt–Fe alloy is intergrown with cooperite, sperrylite and sudburyite (Fig. 4e). Grains of Pt–Fe alloy are dominated by Pt (79.07–83.53 wt.%, 66.22–70.89 at.%) and Fe (5.84–6.09 wt.%, 17.09–18.05 at.%) (Table 3, anal. 11, Table 4, anal. 16). However, other elements detected include Ir (4.87–7.06 wt.%, 4.19–6.00 at.%), Ru (0.64–2.15 wt.%, 1.05–3.48 at.%), Rh (0.81–1.92 wt.%, 1.31–3.05 at.%), Os (0.68–2.02 wt.%, 0.59–1.74 at.%), Pd (0.64–1.13 wt.%, 1.00–1.74 at.%), Cu (0.27–0.97 wt.%, 0.69–2.53 at.%) and Ni (up to 0.14 wt.%, 0.39 at.%). In both cases, the Pt–Fe alloy has an unusual chemical composition that corresponds to an average formula of $PGE_{3.95–4.11}BM_{0.89–1.05}$, close to the stoichiometry PGE_4BM. Formulas of Pt–Fe alloy from grains W3 39 (Fig. 3f) and W1 3–1 (Fig. 4e) can be presented as ($Pt_{3.54}Ir_{0.21}Rh_{0.07}Ru_{0.05}Pd_{0.05}Os_{0.03}$)($Fe_{0.90}Cu_{0.13}Ni_{0.02}$) and ($Pt_{3.31}Ir_{0.30}Rh_{0.15}Ru_{0.17}Os_{0.09}Pd_{0.09}$)($Fe_{0.86}Cu_{0.03}$), respectively.

Sperrylite, $PtAs_2$, occurs as an outer zone on the alloys that usually form the core of polyphase grains (Table 2, Figs. 3a, b, 4). The characteristic feature of the sperrylite in our samples is an enrichment in S (1–1.95 wt.%, 3.19–6.65 at.%), Sb (1.10–1.68 wt.%, 0.92–1.50 at.%), Te (up to 1.04 wt.%, 0.89 at.%), Ni (0.14–1.25 wt.%, 0.39–2.18 at.%), Rh (up to 1.74 wt.%, 1.85 at.%), Co (up to 1.29 wt.%, 2.39 at.%) and Fe (up to 1.00 wt.%, 1.83 at.%) (Table 4, anal. 14, 15, 20–22), which is in contrast to the data presented by Feather (1976).

Laurite, RuS_2, forms inclusions up to 20 μm in Pt–Ir–Os and Pt–Fe alloys (grain W3 39, Fig. 3f). It contains moderate concentrations of both Os (8.83 wt.%, 2.78 at.%) and Ir (4.85 wt.%, 1.51 at.%) with a Ru# corresponding to 91 (Table 4, anal. 17).

Cooperite, PtS, which has been observed in two grains (Table 2, grains W3 39 and W1 3–1) clearly replaces Pt–Fe alloy (Figs. 3f, 4e). It carries notable concentrations of Ru (up to 6.88 wt.%, 6.56 at.%), besides smaller quantities of Rh (up to 3.30 wt.%, 3.09 at.%), Ir (up to 3.49 wt.%, 1.75 at.%), As (up to 2.40 wt.%, 3.09 at.%), Fe (< 0.67 wt.%, 1.16 at.%), Ni (< 0.19 wt.%, 0.35 at.%), Pd (< 0.38 wt.%, 0.42 at.%) and Os (< 0.70 wt.%, 0.35 at.%) (Table 4, anal. 18 and 24).

Other PGM identified are sudburyite, PdSb, and hollingworthite, RhAsS, which appear to be the only minerals of Pd and Rh, respectively, in the PGM nuggets selected (Table 2, Fig. 4e). Sudburyite does not host any detectable trace elements (Table 4, anal. 23), whereas hollingworthite contains considerable contents of Pt (8.78 wt.%, 3.85 at.%), Ru (6.74 wt.%, 5.71 at.%) and Ir (3.97 wt.%, 1.77 at.%), showing common Rh-for-Pt and Rh-for-Ir substitutions and uncommon Rh-for-Ru substitution. Minor elements detected in hollingworthite include Sb (1.56 wt.%, 1.10 at.%), Te (0.61 wt.%, 0.41 at.%), Fe (0.53 wt.%, 0.81 at.%) and Co (0.52 wt.%, 0.76 at.%).

Osmium-Isotope Data

The $^{187}Os/^{188}Os$ values, along with calculated model ages of PGM from Evander, are listed in Table 5 and shown in Figure 6. The $^{187}Os/^{188}Os$ value measured by N–TIMS and LA MC–ICP–MS in PGM grains of different composition (*e.g.,* osmium, ruthenium, rutheniridosmine, Pt–Ir–Os, Ru–Ir–Pt, Ru–Pt and Pt–Fe alloys) was found to range from 0.10987 to 0.1095 (Table 5). Since the concentration of Re in all samples is less than detection limit by EPMA (0.05 wt.%), the isotopic effect resulting from radioactive decay of ^{187}Re *in situ* can be considered to be negligible. Hence, the value of $^{187}Os/^{188}Os$ in the PGM under discussion corresponds to that in the source of the ore material at the time of PGM formation.

The dispersion of the $^{187}Os/^{188}Os$ values in the osmium and ruthenium alloys exceeds the analytical uncertainty. The $^{187}Os/^{188}Os$ value in osmium alloy varies between 0.0987 ± 0.0009 and 0.1061 ± 0.0005; the $^{187}Os/^{188}Os$ value in ruthenium alloy varies from 0.1000 ± 0.0009 to 0.1068 ± 0.0005 (Table 5, Fig. 5, the 2σ errors correspond to the 95% confidence level). The $^{187}Os/^{188}Os$ value in other PGM show a less pronounced variation, over the range from 0.1052 ± 0.0006 to 0.1095 ± 0.0004.

Excluding three PGM nuggets (*i.e.,* W1 3–13, W1 2–18 and W3 28, Table 5, anal. 1–3, Fig. 6A) with the lowest $^{187}Os/^{188}Os$ values (<0.1024) and sample W1 1–7 (Table 5, anal. 13, Fig. 6A) with the highest $^{187}Os/$

^{188}Os value (0.1095), at least two heterogeneous groups of PGM can be identified, with the average ^{187}Os/^{188}Os values of 0.1053 ± 0.0004 (n = 6) and 0.1064 ± 0.0003 (n = 3), respectively (calculation errors are within the 95% confidence level). It is noteworthy that two samples (*i.e.,* W1 3–14 and W1 3–1), which contain the lowest Os contents and thus were measured by LA MC–ICP–MS, show ^{187}Os/^{188}Os values similar to the average numbers (Table 5). However, four values, 0.0987, 0.1000, 0.1024 and 0.1095, are distinctly different (Table 5, Fig. 6). No correlation between chemical composition and isotope content of the samples was discovered within the limits of the experimental precision. Moreover, osmium-isotope ratios in the optically homogeneous PGM crystals range, as a rule, over the same interval as those PGM associations consisting of a core and a rim.

Examples of primary and secondary PGM, which show unradiogenic Os isotope compositions, are represented by the grains W3 39 (Fig. 3f) and W1 3–1 (Fig. 4e). Apart from various primary PGE alloys and laurite, both PGM assemblages contain secondary cooperite, which replaces Pt–Fe alloy. Unradiogenic ^{187}Os/^{188}Os values of PGM from these grains (measured both by N–TIMS and LA MC–ICP–MS) indicate that the system Re–Os in Os-bearing minerals (*i.e.,* Pt–Ir–Os and Pt–Fe alloys) from these assemblages has remained unchanged, despite a secondary overprint. The stability of the osmium-isotope system at the mineral level has also been demonstrated for detrital 3.1–3.4 Ga old gold from the Klerksdorp Goldfield at Witwatersrand (Kirk *et al.* 2001, 2002).

Since the ^{187}Os/^{188}Os values in all PGM analyzed do not exceed the value of the average present-day chon-

TABLE 5. OSMIUM ISOTOPE COMPOSITION AND CALCULATED MODEL AGES OF PGM FROM THE EVANDER GOLDFIELD, WITWATERSRAND

Anal.	Sample	Figure	Main PGM	Atom proportions	^{187}Os/^{188}Os	T_{ch}, Ga
1	W1 3-13	3a, b	Osmium	$(Os_{0.40}Ru_{0.29}Ir_{0.23}Pt_{0.08})$	0.0987(9)	4.104
2	W1 2-18	4a, c	Ruthenium	$(Ru_{0.34}Os_{0.33}Ir_{0.22}Pt_{0.10}Fe_{0.01})$	0.1000(9)	3.931
3	W3 28	3d	Osmium	$(Os_{0.50}Ir_{0.39}Ru_{0.08}Fe_{0.02}Ni_{0.01})$	0.1024(6)	3.611
4	W3 36		Ruthenium	$(Ru_{0.40}Os_{0.38}Ir_{0.17}Pt_{0.02}Fe_{0.02}Rh_{0.01})$	0.1052(4)	3.236
5	W3 39	3f	Pt-Ir-Os alloy	$(Pt_{0.38}Ir_{0.30}Os_{0.17}Fe_{0.07}Ru_{0.06}Rh_{0.02})$	0.1052(6)	3.236
6	W3 37		Osmium	$(Os_{0.35}Ir_{0.34}Ru_{0.27}Rh_{0.02}Fe_{0.01}Pt_{0.01})$	0.1053(6)	3.222
7	W1 3-14	4b, d, f	Ru-Ir-Pt alloy	$(Ru_{0.38}Ir_{0.28}Pt_{0.21}Os_{0.07}Fe_{0.06})$	0.1053(8)	3.222
8	W1 2-2	3c	Osmium	$(Os_{0.34}Ru_{0.31}Ir_{0.26}Pt_{0.07}Fe_{0.01}Ni_{0.01})$	0.1054(8)	3.209
9	W3 33		RIO[1]	$(Ir_{0.36}Os_{0.33}Pt_{0.14}Ru_{0.13}Fe_{0.04})$	0.1055(4)	3.196
Average 1 (analyses 4 to 9; n = 6)					0.1053	3.222
10	W3 60		Osmium	$(Os_{0.50}Ir_{0.39}Ru_{0.08}Fe_{0.02}Ni_{0.01})$	0.1061(5)	3.115
11	W1 3-1	4e	Pt-Fe alloy	$(Pt_{0.66}Fe_{0.17}Ir_{0.06}Ru_{0.03}Rh_{0.03}Os_{0.02}Pd_{0.02})$	0.1063(9)	3.088
12	W1 1-4	3e	Ruthenium	$(Ru_{0.43}Os_{0.19}Ir_{0.19}Pt_{0.13}Fe_{0.05}Ni_{0.01})$	0.1068(5)	3.020
Average 2 (analyses 10 to 12; n = 3)					0.1064	3.074
13	W1 1-7		Ru-Pt alloy	$(Ru_{0.69}Pt_{0.15}Ir_{0.08}Os_{0.07}Fe_{0.01})$ Allègre & Luck (1980)	0.1095(4)	2.655
14	-		"Osmiridium"	- Malitch *et al.* (2000)	0.1084(50)[2]	2.804
15	W1 2-12		Osmium	$(Os_{0.47}Ir_{0.26}Ru_{0.20}Pt_{0.06}Fe_{0.01})$	0.1050(4)	3.263
16	W2 1-8		Osmium	$(Os_{0.65}Ir_{0.33}Ru_{0.02})$	0.1050(5)	3.263
17	W1 2-3		Ru-Ir-Pt alloy	$(Ru_{0.50}Ir_{0.27}Pt_{0.14}Os_{0.06}Fe_{0.03})$	0.1054(3)	3.209
18	W3 15		Osmium	$(Os_{0.58}Ir_{0.36}Ru_{0.05}Fe_{0.01})$	0.1056(3)	3.182
19	W2 1-2	2a, b	Iridium	$(Ir_{0.63}Os_{0.33}Ru_{0.03}Fe_{0.01})$	0.1057(5)	3.169
Average 1 (analyses 15 to 19; n = 5)					0.1053	3.222
20	W2 2-5		Ruthenium	$(Ru_{0.41}Os_{0.21}Pt_{0.17}Ir_{0.16}Fe_{0.04}Ni_{0.01})$	0.1062(3)	3.101
21	W3 27		Osmium	$(Os_{0.42}Ir_{0.32}Ru_{0.18}Pt_{0.06}Fe_{0.01}Ni_{0.01})$	0.1063(3)	3.088
22	W2 2-3	2c, d	RIO[1]	$(Ir_{0.32}Ru_{0.26}Os_{0.22}Pt_{0.15}Fe_{0.05})$	0.1064(4)	3.074
23	W2 2-1		Osmium	$(Os_{0.49}Ir_{0.41}Ru_{0.09}Fe_{0.01})$	0.1066(4)	3.047
24	W1 2-1		Osmium	$(Os_{0.33}Ru_{0.31}Ir_{0.26}Pt_{0.08}Fe_{0.01}Ni_{0.01})$	0.1068(3)	3.020
Average 2 (analyses 20 to 24; n = 5)					0.1065	3.060
25	W2 2-6		Osmium	$(Os_{0.55}Ir_{0.41}Fe_{0.02}Pt_{0.01}Ni_{0.01})$	0.1072(7)	2.966
26	W1 2-4	2e, f	Osmium	$(Os_{0.36}Ru_{0.32}Ir_{0.23}Fe_{0.06}Ni_{0.02}Pt_{0.01})$	0.1091(4)	2.709

Entries 1–6, 8–10 and 12: N-TIMS analyses; 7, 11 and 13: LA MC–ICP–MS analyses; [1]RIO: rutheniridosmine; [2] recalculated (^{187}Os/^{188}Os = ^{187}Os/^{186}Os multiplied by 0.12035). Numbers in parentheses express 2σ uncertainty in the last decimal places of the ^{187}Os/^{188}Os values. Model ages were calculated with CHUR values estimated by Chen *et al.* (1998) and a ^{187}Re decay constant of $\lambda = 1.666E^{-11}$ y^{-1} (Smoliar *et al.* 1996).

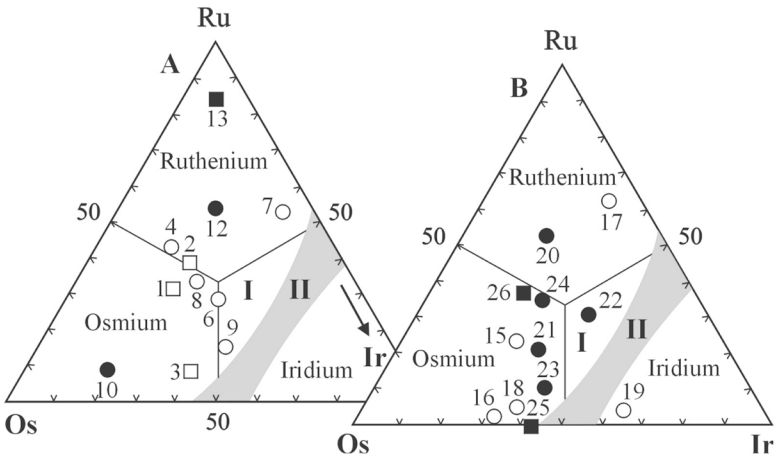

FIG. 6. Composition of detrital Ru–Os–Ir alloys at Evander in terms of the diagram Ru – Os – Ir, at.%. Fields I and II: rutheniridosmine and miscibility gap, respectively. IPGE alloy grains measured by N–TIMS and LA MC–ICP–MS (A, this study) and by N–TIMS (B, Malitch *et al*. 2000). IPGE alloys were subdivided according to their osmium-isotope composition; open squares: PGM with $^{187}Os/^{188}Os$ less than 0.1024, open circles: $^{187}Os/^{188}Os$ in the range 0.1050–0.1057, filled circles: $^{187}Os/^{188}Os$ in the range 0.1061–0.1068, filled squares: $^{187}Os/^{188}Os$ in the range 0.1072–0.1095. Numbers 1–13, 15–26 correspond to the same numbers in Table 5.

dritic uniform reservoir (CHUR) (0.12863 ± 0.00046, Chen *et al.* 1998), a model Re–Os age can be calculated according to the method of Allègre & Luck (1980). A number of assumptions must be fulfiled if the calculated ages are to be meaningful. In order to calculate model $^{187}Os/^{188}Os$ ages of PGM, the $^{187}Os/^{188}Os$ evolution curve of the CHUR has to be known and constrained by initial and present-day $^{187}Os/^{188}Os$ values. In this study, we use the initial and present-day $^{187}Os/^{188}Os$ values (0.0953 ± 0.0013 and 0.12863 ± 0.00046, respectively) along with the present-day $^{187}Re/^{188}Os$ value (0.423 ± 0.007) as estimated by Chen *et al.* (1998). Alternative $^{187}Os/^{188}Os$ values for the present-day mantle in widespread use for the calculation of model ages are 0.12736 (Yin *et al*. 1996), 0.1270 (Shirey & Walker 1998) and 0.1296 ± 0.0008 (Meisel *et al.* 2001), whereas the $^{187}Re/^{188}Os$ value is taken to be equal to 0.40186 by Shirey & Walker (1998). Calculations using the first two estimates of $^{187}Os/^{188}Os$ would result in model ages that are approximately 0.15–0.2 Ga younger. If the $^{187}Os/^{188}Os$ value of primitive upper mantle (PUM; Meisel *et al*. 2001) is used, the model ages of PGM are approximately 0.2 Ga older. However, as is clear from recent *in situ* studies on base-metal sulfides (Alard *et al*. 2002), the estimate of the PUM of Meisel *et al.* (2001) derived from bulk geochemical studies of xenoliths cannot be used as a valid proxy material for mantle PGM.

The Re/Os value of the Earth as a whole (*i.e.,* Bulk Earth) and, in particular, that of the mantle, has not changed during the 4.56 Ga of geological history, which allows the assumption that mantle-derived $^{187}Os/^{188}Os$ ages for derivatives of mantle origin are close to real ones in comparison to similar ratios for the other isotope systems. This statement is particularly true for Re-free Os-rich mantle minerals, because their ages cannot be overestimated (see for details Kirk *et al.* 2002, p. 2154). Underestimation of ages is also unlikely, as the Re–Os isotope system at the crystal-scale level is well protected against crustal contamination, as has been demonstrated for Ru–Os sulfides from variably altered chromitites at Kraubath, Austria (Malitch *et al.* 2003a).

On the basis of the osmium-isotopic composition of Ru–Os–Ir and Pt–Fe alloys, model $^{187}Os/^{188}Os$ ages range from 4.104 to 2.655 Ga (Table 5). The two PGM groups mentioned above have average model $^{187}Os/^{188}Os$ ages of 3.222 ± 0.078 Ga and 3.074 ± 0.060 Ga, respectively (Table 5, anal. 4–12). The model $^{187}Os/^{188}Os$ ages of other four PGM grains (*i.e.,* W1 3–13, W1 2–18, W3 28 and W1 1–7) are distinctly different (4.104, 3.931, 3.611 and 2.655 Ga, respectively) (Table 5, anal. 1–3 and 13).

The isotopic composition of osmium in the osmium alloys yield model $^{187}Os/^{188}Os$ ages in the range of 4104 Ma to 3115 Ma, which is indistinguishable from the total variation defined by ruthenium alloys (*i.e.,* 3931–3020 Ma: Table 5, Fig. 6). In contrast, model $^{187}Os/^{188}Os$ ages for PGM grains with secondary cooperite vary between 3222 and 3088 Ma only (Table 5, anal. 7 and 11, Fig. 6). The Os isotope system thus has not been disturbed during later thermal events, which affected the

Witwatersrand Basin at 2550, 2300 and over the interval 2020–2060 Ma (Robb & Meyer 1995, Stevens *et al*. 1997).

Discussion

Mineralogical and osmium isotope constraints for genesis of the PGE mineralization

In their mineralogical studies, Barrass (1974) and Feather (1976) reported that Os–Ir–Ru alloys [osmium and iridium according to the presently applied nomenclature of Harris & Cabri (1991)] are the most common group of PGM (60–90%), followed by Pt–Fe alloy (5–10%), sperrylite (5–10%) and various other subordinate PGM in a range of <1–3%. Quantitative electron-microprobe analyses, however, imply that the PGM grains from the Evander Goldfield may differ systematically in their composition from the PGM in the rest of the Witwatersrand Basin (Merkle & Franklyn 1999, Malitch *et al*. 2000), a feature supported by more recent analyses (Figs. 2, 5, Tables 1–4). This difference indicates the existence of a variety of source regions for the Witwatersrand Basin.

Many of the alloys are mantled by sulfides, arsenides and sulfarsenides of PGE (Feather 1976, Merkle & Franklyn 1999, this study), whereas the cores of such mineralogically zoned grains are very variable, from optically homogeneous to very complex intergrowths and "replacement" textures. In PGM from placer deposits, certain textures have been interpreted as due to replacement (Feather 1976, Stumpfl & Tarkian 1976, Cabri *et al*. 1996, Merkle & Franklyn 1999), especially if they follow distinct crystallographic directions. Such replacements involve either removal or addition of a specific element (like arsenic) at a lower temperature than the temperature of formation of the original grain, and may consequently represent a younger age.

Following earlier interpretations of textures in PGM grains from the Witwatersrand Basin (Feather 1976, Stumpfl & Tarkian 1976, Toma & Murphy 1978), one could propose that the homogeneous core of the alloy grains represents abraded material, which was overgrown at a later stage, at a lower temperature, possibly after deposition in the Witwatersrand Basin. We have not yet seen any undoubtedly high-temperature or weathering-prone inclusions in the "overgrowth" zones that would exclude such an interpretation. However, the mineralogy of the rim material and the extremely low concentrations of PGE in the Witwatersrand reefs, combined with the low solubility of the PGE in hydrous fluids (Mountain & Wood 1988) and the short distances of transport (mm to cm) implied for the more soluble gold (Frimmel & Minter 1991), make this a very unlikely option for the formation of the As-containing zones around PGM grains (Feather & Koen 1975, Feather 1976, Oberthür 1983). The rims of cooperite observed in our study represent a replacement feature and thus may be interpreted as secondary.

The unusual diversity of polycomponent alloys of the system Ru–Os–Ir–Pt(±Fe) observed in this study (Fig. 2) and previously by Merkle & Franklyn (1999) and Malitch *et al.* (2000) is in basic accordance with the fractionation trend proposed by Feather (1976). On the basis of Figure 7 (after Okrugin 2002), it is obvious that the compositions of some of the PGE alloys from the Witwatersrand that plot near the Os corner imply temperatures of formation in excess of 1000°C, whereas the Ir-rich compositions imply maximum temperatures of formation in excess of 850°C. Although these isotherms (dashed lines) are extrapolated and should not be taken as quantitative evidence, they imply conditions of formation that are above the temperatures typically considered to represent hydrothermal environments. A substantial number of compositions plot in an area which, according to the extrapolated phase-relations, should not exist as a homogeneous alloy at subsurface pressures. If one does not assume that they were actually molten metals at temperatures above the liquidus isotherms (stippled lines), then it has to be assumed that phase-boundary shifts due to increased pressure are responsible for allowing such compositions. Although we can only speculate about the effect of pressure, a substantial reduction of the miscibility gap in this ternary system would imply a substantial depth of formation, again excluding a hydrothermal mode of formation.

Equilibrium phase-relationships of osmium and ruthenium alloys at Evander, based on the restricted solid-solution in the binary systems Os–Ir, Os–Ru and Ir–Ru (Massalski 1993), and the presence of a ruthenium-enrichment trend in Os–Ru–Ir–Pt alloys, are indicative of high temperatures and pressures, which could only be reached under mantle conditions (Bird & Bassett 1980, Malitch & Badanina 1998). We therefore propose that these PGM likely represent examples of slightly differentiated PGE alloys, which were formed in the Archean mantle.

Since the pioneering work by Allègre & Luck (1980), the investigations on the Re–Os systematics of PGM have been mainly conducted on PGM from placers derived from Phanerozoic dunite–harzburgite (of Alpine or ophiolite type) or clinopyroxenite–dunite (zoned, Uralian or Alaskan type) massifs (Hattori & Hart 1991, Hattori *et al.* 1992, Hattori & Cabri 1992, Hirata *et al*. 1998, Bird *et al*. 1999, Malitch *et al*. 2002a, b, among others); these examples show that the PGM formed in close association with ultramafic rocks. The possibility of high-temperature formation of Ru–Os sulfides and Os–Ru–Ir alloys has been confirmed experimentally (Andrews & Brenan 2002), which implies that the Os isotopic composition of Ru–Os sulfides and Ru–Os–Ir alloys should reflect that of the source region from which they formed. The low, "unradiogenic" $^{187}Os/^{188}Os$ values of PGM at Evander (Table 5, Fig. 6) clearly

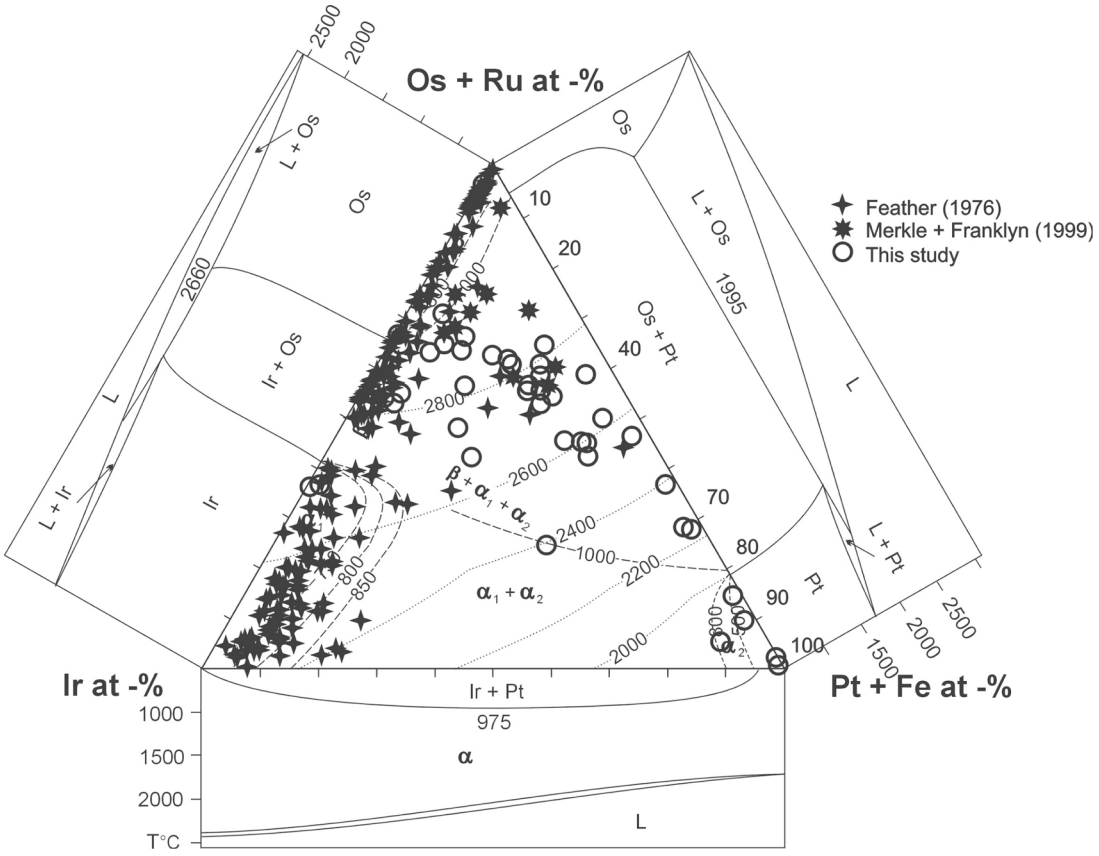

FIG. 7. Compositions of Os(+Ru)–Ir–Pt(+Fe) alloys from Evander in relation to extrapolated phase-relations in the system Os(+Ru)–Ir–Pt(+Fe) after Okrugin (2002). Dashed lines are stability limits at the indicated temperatures; stippled lines are isotherms on the liquidus.

indicate a chondritic to subchondritic mantle source for the PGE. Consequently, the PGM were formed during mantle melting in the Archean mantle environment without any significant crustal contribution of Os; the $^{187}Os/^{188}Os$ values show no evidence of change by subsequent processes such as transport, sedimentation and weathering during placer formation, and subsequent metamorphism of the Witwatersrand Basin.

The high stability of the osmium-isotope system within PGM is further confirmed by two grains (W3 39 and W3 3–1) that contain secondary cooperite attributed to later overprinting events. If the Re–Os system had been perturbed, then these PGM should have yielded the most radiogenic values. However, these PGM grains fall within the range of unradiogenic $^{187}Os/^{188}Os$ values obtained in this study. The Os isotope compositions of PGM from Evander correspond to that estimated for the Archean mantle, which has low $^{187}Os/^{188}Os$ values as a result of evolution in a low-(Re/Os) environment (Shirey & Walker 1998).

Os isotopic constraints for timing of PGM formation

The $^{187}Os/^{188}Os$ values obtained by Malitch *et al.* (2000) and in this study appear to be consistent with the recalculated osmium-isotope values of Hart & Kinloch (1989), based on PGM from the Welkom Goldfield in the south of the Witwatersrand Basin. According to these calculations, the PGM from the Welkom Goldfield may be divided into three groups, implying ages of 3210, 3070 and 2820 Ma, respectively. Therefore, some ages of PGM from the Welkom Goldfield appear to be close to those of the Evander Goldfield (*i.e.,* 3222 and 3074 Ma, respectively), despite the wider range of model ages of the Welkom suite (Table 5).

The oldest model $^{187}Os/^{188}Os$ ages at the Evander Goldfield (Table 5, anal. 1–3) were obtained for (1) rounded polyphase PGM grains, which consist of osmium alloy $Os_{0.40}Ru_{0.29}Ir_{0.23}Pt_{0.08}$ (*i.e.,* W1 3–13) and ruthenium alloy, $Ru_{0.35}Os_{0.32}Ir_{0.22}Pt_{0.10}Fe_{0.01}$ (W1 2–18), both mantled by sperrylite, and (2) a monophase hex-

agonal crystal (W3 28) with an approximate formula $Os_{0.50}Ir_{0.39}Ru_{0.08}Fe_{0.02}Ni_{0.01}$. These findings are likely to represent the oldest known terrestrial PGM, originating in the Early Archean.

The provenance of the detrital material in the Witwatersrand Basin from a varied hinterland with distinct ages is also reflected by extensive geochronological data that were obtained through U–Pb dating of zircon from conglomerates of various stratigraphic levels (Barton *et al*. 1989, Robb *et al*. 1990, Armstrong *et al*. 1991, Poujol *et al*. 1999). Variations in U–Pb ages of zircon very likely reflect episodes of felsic magmatic activity during the period 3300–2900 Ma, when extensive formation of granite occurred. Kirk *et al.* (2002) provided osmium-isotopic evidence that the gold and rounded pyrite from the conglomerate horizons also are of detrital origin. These minerals yield a Re–Os isochron age of 3.03 ± 0.02 Ga with an initial $^{187}Os/^{188}Os$ ratio of 0.1079 ± 0.0001 (Kirk *et al*. 2002), indicating that significant flux of noble metals from mantle sources took place in the Middle Archean. The Rb–Sr isotope system allows the detection of late metamorphic processes, which occurred at 2550, 2300, and over the interval 2020–2060 Ma (Robb & Meyer 1995, Stevens *et al*. 1997). In this context, the model osmium-isotope ages obtained for the main set of the PGM (4104–3020 Ma) favor a scenario in which PGM originated from as yet unknown mafic–ultramafic complexes of similar ages, derived from a chondritic mantle, and not deposited or mobilized by later hydrothermal fluids. The only exception observed so far is a Ru–Pt alloy (grain W1 1–7, Table 5, anal. 13), with a model $^{187}Os/^{188}Os$ age possibly somewhat younger (2.655 ± 0.050 Ga) than the time of deposition of the Central Rand Group sediments (*i.e.,* 2.940–2.710 Ga). This Ru–Pt alloy could be interpreted as having been derived from a crustal source.

Comparison of Re–Os dating of PGM and U–Pb dating of zircon (Fig. 8) provides reasonable evidence of close relationships between magmatic and ore-forming processes. The average age of zircon older than 2.500 Ga is 3.032 Ga (90% confidence interval: 3.009 to 3.055 Ga), close to the average model $^{187}Os/^{188}Os$ age of 3.118 Ga (90% confidence interval: 3.055 to 3.190 Ga).

Implications for the source area

The heavy minerals (*e.g.,* gold, PGM, chromite, zircon) in the Witwatersrand Basin suggest that the source regions for the detritus must have been a mixture of granitic rocks, hydrothermal veins, and mafic to ultramafic rocks. However, many of the petrological characteristics of these source rocks, their volume proportions, and their paleogeographic position are poorly defined (Reimer 1979, Hutchison & Viljoen 1988, Robb & Meyer 1990, Pretorius 1991, Venneman *et al*. 1996, among others). The dominance of Os–Ru–Ir alloys over other PGM, as recorded at Witwatersrand, is not unusual in mantle sections of dunite–harzburgite complexes. In fact, it is considered a typical feature of PGE occurrences in Phanerozoic dunite–harzburgite complexes worldwide (Cabri & Harris 1975, Legendre & Augé 1986, Palandzhian *et al*. 1994, Cabri *et al.* 1996, Melcher *et al.* 1997). However, the assemblage of PGM at Evander does not match that expected in Phanerozoic ophiolites. It may thus be that ophiolites in Archean were characterized by a greater diversity of PGM assemblages.

Cousins (1973) has argued that the relatively high bulk (Os + Ir)/(Ru + Pt + Rh) value reflects placer maturity in the Witwatersrand Basin. However, taking into account the apparent consistency of the mineralogy, the rather constant PGE ratios along strike and down dip, the inert character of most of the PGM identified (Feather 1976), and the short distance from the shoreline compared to the inferred distances of transport from the hinterland, the proportions of PGM in the Witwatersrand Basin must consistently reflect the petrological characteristics of the hinterland. Besides, even PGM containing Sb and Te, which are considered to be very prone to alteration and destruction, have been observed (Feather 1976, this study), which implies that the maturity of the placers has been overestimated.

In the Witwatersrand Basin as a whole, the proportions of Pt–Fe alloy and of sperrylite in the PGM concentrates were estimated to be 5–10 volume % each (Feather 1976). Such a proportion of Pt-dominant minerals seems far too low to assume a purely zoned-type source (Rozhkov *et al*. 1962, Barron *et al*. 1990, Nixon *et al*. 1990, Cabri & Genkin 1991, Cabri *et al*. 1996, Malitch 1999, Garuti *et al*. 2002, Johan 2002) and even too low for many ophiolites (Cabri & Harris 1975,

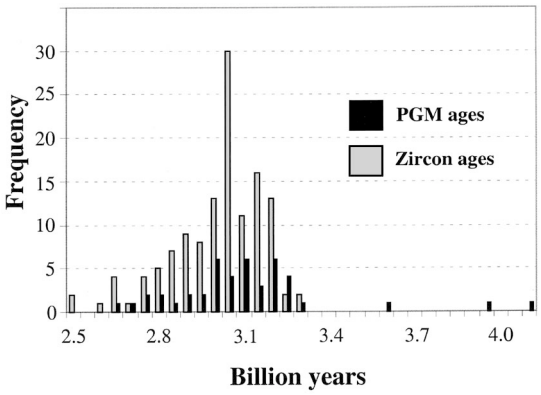

FIG. 8. Comparison of model $^{187}Os/^{188}Os$ ages of PGM (Allègre & Luck 1980, Hart & Kinloch 1989, Malitch *et al*. 2000, this study) with U–Pb zircon ages (Armstrong *et al*. 1991, Barton *et al*. 1989, Robb *et al*. 1990) in deposits of the Witwatersrand Basin.

Legendre & Augé 1986, Melcher *et al*. 1997, Augé *et al*. 1998, Malitch *et al*. 2003b). However, most of these occurrences are relatively young, and direct comparison is likely not valid, since PGE speciation may have been slightly different in the Archean. In addition, the variability among PGM within the same geological body, as well as the discrepancy between PGM from bedrocks and placers, have frequently been pointed out (Barron *et al*. 1990, Nixon *et al*. 1990, Cabri & Genkin 1991, Augé & Maurizot 1995). Nevertheless, there are examples of placers with a very low Pt:(Os + Ir) ratio. The placers in Tasmania are dominated by Os- and Ir-rich PGM and are considered to be derived from a dunite–harzburgite complex of Cambrian age (Cabri & Harris 1975, Peck *et al*. 1992, Cabri *et al*. 1996). Incidentally, the composition of silicate inclusions in these PGM is consistent with the model that crystallization occurred in the lithospheric upper mantle (Peck *et al*. 1992).

The Guli ultramafic massif in northern Siberia (Butakova 1974, Malitch & Lopatin 1997, Malitch *et al*. 2002a) is atypical in several respects. Although some placers associated with this massif contain an Os–Ir–Ru-dominant assemblage, the huge size of the Guli Complex, ~2000 km^2, with an exposed area of >500 km^2 of clinopyroxenite–dunite, place it in a totally different category compared to more typical sizes of Aldan-type clinopyroxenite–dunite complexes or the ~30 km^2 of Kondyor and ~22 km^2 of Inagli (Rozhkov *et al*. 1962, Malitch 1999).

The Os–Ir–Ru dominance of the Witwatersrand placers implies that an "ophiolitic" source was dominant. However, owing to the cover by younger Karoo rocks, no evidence is available about the possible presence of ophiolites to the southwest of the Evander Goldfield. The 3.3–3.5 Ga "Jamestown ophiolite" (De Wit *et al*. 1987) in the Barberton greenstone belt, to the southeast, has recently been shown to be a misinterpretation (Anhaeusser 2001).

The Murchison Greenstone Belt, on the northeast of the Kaapvaal craton, dated at 3070–2970 Ma (Poujol *et al*. 1996), can be considered as a possible source of the PGM documented here. However, there seems to be no confirmed record of PGM in any of the South Africa greenstone belts (Wagner 1973), and there is also no information available on the mineralogical expression of any elevated PGE levels in other South African greenstone belts of suitable age (De Wit & Tredoux 1988).

Finally, the only environments from which placers with proportions of PGM similar to those in the Witwatersrand have been described, and where the geological environment is reasonably well constrained, are in the Tasmanian example cited above and possibly Guli (northern Siberia). In order to consider either of these rocks from the lithospheric upper mantle (like in the Heazlewood River Complex of Tasmania) or special cases of clinopyroxenite–dunite complexes like Guli, in northern Siberia, as the main source for the PGM in the Witwatersrand basin, their tectonic emplacement and exposure prior to sedimentation in the Witwatersrand Basin have to be considered. However, no suitable deep-seated structures are known at present in the likely source-regions to the north and south of the basin.

Conclusions

1. Grains of Ru–Os–Ir–Pt and Pt–Fe alloys from the Evander Goldfield, situated in the eastern part of the Witwatersrand Basin, South Africa, have been studied by a number of modern techniques (SEM, EMPA, N–TIMS and LA MC–ICP–MS).

2. The characteristic feature of PGM from Evander is a common occurrence of compositionally distinct Ru-rich alloys (*i.e.,* Ru–Os–Ir, Ru–Os–Ir–Pt, Ru–Ir–Pt, Ru–Pt), which prevail over osmium, iridium, ruthenium, iridosmine, Pt–Fe, Pt–Ru–Fe and Pt–Ir–Os alloys and other PGM. Osmium-bearing PGM occur as (a) single grains and (b) complex polyphase assemblages.

3. The $^{187}Os/^{188}Os$ value measured by N–TIMS in ten PGM grains, which contain Os in the range 18–53 wt.% (*i.e.,* Pt–Ir–Os alloy, ruthenium, ruthenium iridosmine and osmium), was found to range from 0.0987 to 0.1068, revealing the lowest three $^{187}Os/^{188}Os$ values (0.0987–0.1024) reported so far in terrestrial PGM. The $^{187}Os/^{188}Os$ ratio measured by LA MC–ICP–MS in PGM with Os contents between 2 and 10 wt.% (*i.e.,* Pt–Fe, Ru–Ir–Pt and Ru–Pt alloys) varies from 0.1053 to 0.1095. $^{187}Os/^{188}Os$ values measured by N–TIMS and LA MC–ICP–MS are clearly indicative of a chondritic to subchondritic mantle source of the PGE.

4. For the major set of PGM (n = 9), independently of their chemical composition, two groups of isotopic values were distinguished. The mean $^{187}Os/^{188}Os$ value for the first group amounts to 0.1053 ± 0.0002, whereas that of the second group is 0.1064 ± 0.0004, which is in good agreement with earlier findings (Hart & Kinloch 1989, Malitch *et al*. 2000). Accordingly, estimates of age based on the mean osmium-isotopic composition of PGE alloys yielded model $^{187}Os/^{188}Os$ ages of 3222 ± 78 and 3074 ± 60 Ma. Three PGM, however, appear to imply ages of 4100 ± 130, 3930 ± 130 and 3610 ± 85 Ma, respectively, representing the oldest terrestrial PGM known so far.

5. The compositional and geochemical-isotopic data obtained imply that the source for the PGM was the Archean mantle, slightly differentiated with respect to PGE. We further propose that the PGM formed under mantle conditions. Finally, our results support a scenario in which the majority of PGM were incorporated into the Witwatersrand Basin as detrital material, derived most probably from Archean ultramafic rocks of yet unidentified affinity.

Acknowledgements

This is a contribution for IGCP Project 479. The financial support of this study by the Ministry of Natural Resources of Russian Federation, Committee of Natural Resources of Taimyr Autonomous District (Noril'sk, Russia) through project 98/6–H to K.N.M. is gratefully acknowledged. We are indebted to Billiton South Africa, in particular Dr. Pierre Hofmeyr, for supplying the PGM concentrate, to Dr. Stephan A. Junk, Dr. Anatoly I. Kostoyanov, Helmut Mühlhans, Prof. Ernst Pernicka and Prof. Nikolai S. Rudashevsky for valuable analytical assistance, and to Dr. Steve Prevec and an unidentified reviewer for criticism and constructive comments. The completion of this study would have not been possible without the financial support by Mining University of Leoben through a Guest Professorship to K.N.M. during 2003. Stimulating discussions with members of the Department of Mineralogy and Petrology, Institute of Geological Sciences, Mining University of Leoben are greatly appreciated. Finally, we express our gratitude to Robert F. Martin for his thorough and significant editorial input.

References

Alard, O., Griffin, W.L., Pearson, N.J., Lorand, J.-P. & O'Reilly, S.Y. (2002): New insights into the Re–Os systematics of sub-continental lithospheric mantle from in situ analysis of sulphides. *Earth Planet. Sci. Lett.* **203**, 651-663.

Allègre, C.J. & Luck, J.-M. (1980): Osmium isotopes as petrogenetic and geological tracers. *Earth Planet. Sci. Lett.* **48**, 148-154.

Andrews, D.R.A. & Brenan, J.M. (2002): Phase-equilibrium constraints on the magmatic origin of laurite + Ru–Os–Ir alloy. *Can. Mineral.* **40**, 1705-1716.

Anhaeusser, C.R. (2001): The anatomy of an extrusive-intrusive Archaean mafic-ultramafic sequence: the Nelshoogte Schist Belt and Stolzburg Layered Ultramafic Complex, Barberton Greenstone Belt, South Africa. *S. Afr. J. Geol.* **104**, 167-204.

Armstrong, R.A., Compston, W., Retief, E.A., Williams, I.S. & Welke, H.J. (1991): Zircon ion microprobe studies bearing on the age and evolution of the Witwatersrand triad. *Precamb. Res*. **53**, 243-266.

Augé, T., Legendre, O. & Maurizot, P. (1998): The distribution of Pt and Ru–Os–Ir minerals in the New Caledonia Ophiolite. *In* International Platinum (N.P. Laverov & V.V. Distler, eds.). Theophrastus Publications, St. Petersburg, Russia (141-154).

_____ & Maurizot, P. (1995): Stratiform and alluvial platinum mineralization in the New Caledonia ophiolite complex. *Can. Mineral*. **33**, 1023-1045.

Barrass, P.F. (1974): *Platinoid Minerals in the Gold Reefs of the Witwatersrand Basin*. M.Sc. thesis, Durham University, Durham, U.K.

Barron, L.M., Slansky, E., Johan, Z. & Ohnenstetter, M. (1990): Fifield placer mineralogy: the key to the source rocks. *In* Placer Deposits: a Symposium (M. Noakes, ed.). Austral. Inst. Mining Metall., Sydney, Australia (89-98).

Barton, E.S, Compston, W., Williams, I.S., Bristow, J.W., Hallbauer, D.K. & Smith, C.B. (1989): Provenance ages for the Witwatersrand supergroup and the Ventersdorp contact reef: constraints from ion microprobe U–Pb ages of detrital zircons. *Econ. Geol*. **84**, 2012-2019.

Bird, J.M. & Bassett, W.A. (1980): Evidence of a deep mantle history in terrestrial osmium – iridium – ruthenium alloys. *J. Geophys. Res.* **85**, 5461-5470.

_____, Meibom, A., Frei, R. & Nägler, T.F. (1999): Osmium and lead isotopes of rare OsIrRu minerals: derivation from the core–mantle boundary region? *Earth Planet. Sci. Lett.* **170**, 83-92.

Butakova, E.L. (1974): Regional distribution and tectonic relations of the alkaline rocks of Siberia. *In* The Alkaline Rocks (H. Sørensen, ed.). John Wiley & Sons Ltd., London, U.K. (172-189).

Cabri, L.J. & Genkin, A.D. (1991): Re-examination of Pt alloys from lode and placer deposits, Urals. *Can. Mineral*. **29**, 419-425.

_____ & Harris, D.C. (1975): Zoning in Os–Ir alloys and the relation of the geological and tectonic environment of the source rocks to the bulk Pt:Pt + Ir + Os ratio for placers. *Can. Mineral.* **13**, 266-274.

_____, _____ & Weiser, T.W. (1996): Mineralogy and distribution of platinum-group mineral (PGM) placer deposits of the world. *Explor. Mining Geol.* **5**, 73-167.

Chen, J.H., Papanastassiou, D.A. & Wasserburg, G.J. (1998): Re–Os systematics in chondrites and the fractionation of the platinum-group elements in the early solar system. *Geochim. Cosmochim. Acta* **62**, 3379-3392.

Cousins, C.A. (1973): Platinoids in the Witwatersrand system. *J. S. Afr. Inst. Mining Metall.* **73**, 184-199.

Creaser, R.A., Papanastassiou, D.A. & Wasserburg, G.J. (1991): Negative thermal ion mass spectrometry of osmium, rhenium, and iridium. *Geochim. Cosmochim. Acta* **55**, 397-401.

De Wit, M.J., Hart, R.A. & Hart, R.J. (1987): The Jamestown ophiolite complex, Barberton mountain belt: a section through 3.5 Ga oceanic crust. *J. Afr. Earth Sci.* **5**, 681-730.

_____ & Tredoux, M. (1988): PGE in the 3.5 Ga Jamestown ophiolite complex, Barberton greenstone belt, with

implications for PGE distribution in simatic lithosphere. *In* Geoplatinum 87 (H.M. Prichard, P.J. Potts, J.F.W. Bowles & S.J. Cribb, eds.). Elsevier, Essex, U.K. (319-341).

DU TOIT, A.L. (1954): *Geology of South Africa* (3rd ed.). Oliver & Boyd, Edinburgh, U.K.

FEATHER, C.E. (1976): Mineralogy of platinum-group minerals in the Witwatersrand, South Africa, *Econ. Geol.* **71**, 1399-1428.

_____ & KOEN, G.M. (1975): The mineralogy of the Witwatersrand reefs. *Minerals Science and Engineering* **7**, 189-224.

FRIMMEL, H.E., HALLBAUER, D.K. & GARTZ, V.H. (1999): Gold-mobilising fluids in the Witwatersrand Basin: composition and possible sources. *Mineral. Petrol.* **66**, 55-81.

_____ & MINTER, W.E.L. (1991): The mobility of Witwatersrand gold during post-depositional alteration. *In* Source, Transport and Deposition of Metals (M. Pagel & J.L. Leroy, eds.). Balkema, Rotterdam, The Netherlands (657-660).

GARUTI, G., PUSHKAREV, E.V. & ZACCARINI, F. (2002): Composition and paragenesis of Pt alloys from chromitites of the Uralian – Alaskan-type Kytlym and Uktus complexes, northern and central Urals, Russia. *Can. Mineral.* **40**, 357-376.

HARRIS, D.C. & CABRI, L.J. (1991): Nomenclature of platinum-group-element alloys: review and revision. *Can. Mineral.* **29**, 231-237.

HART, S.R. & KINLOCH, E.D. (1989): Osmium isotope systematics in Witwatersrand and Bushveld ore deposits. *Econ. Geol.* **84**, 1651-1655.

HATTORI, K., BURGATH, K.-P. & HART, S.R. (1992): Os-isotope study of platinum-group minerals in chromitites in Alpine-type ultramafic intrusions and the associated placers in Borneo. *Mineral. Mag.* **56**, 157-164.

_____ & CABRI, L.J. (1992): Origin of platinum-group-mineral nuggets inferred from an osmium-isotope study. *Can. Mineral.* **30**, 289-301.

_____ & HART, S.R. (1991): Osmium-isotope ratios of platinum-group minerals associated with ultramafic intrusions: Os-isotopic evolution of the oceanic mantle. *Earth Planet. Sci. Lett.* **107**, 499-514.

HIRATA, T., HATTORI, M. & TANAKA, T. (1998): In-situ osmium isotope ratio analyses of iridosmines by laser ablation – multiple collector – inductively coupled plasma mass spectrometry. *Chem. Geol.* **144**, 269-280.

HUTCHISON, R.W. & VILJOEN, R.P. (1988): Re-evaluation of gold source in Witwatersrand ores. *Geol. Soc. S. Afr., Trans.* **91**, 157-173.

JOHAN, Z. (2002): Alaskan-type complexes and their platinum-group element mineralization. *In* The Geology, Geochemistry, Mineralogy and Beneficiation of Platinum-Group Elements (L.J. Cabri, ed.). *Can. Inst. Mining, Metall. Petroleum, Spec. Vol.* **54**, 669-719.

JUNK, S.A. (2001): Ancient artefacts and modern analytical techniques – usefulness of laser ablation ICP–MS demonstrated with ancient gold coins. *Nucl. Instrum. Methods Phys. Res.* **B 181**, 723-727.

KIRK, J., RUIZ, J., CHELSEY, J., TITLEY, S. & WALSHE, J. (2001): A detrital model for the origin of gold and sulfides in the Witwatersrand basin based on Re–Os isotopes. *Geochim. Cosmochim. Acta* **65**, 2149-2159.

_____, _____, _____, WALSHE, J. & ENGLAND, G. (2002): A major Archean, gold- and crust-forming event in the Kaapvaal Craton, South Africa. *Science* **297**, 1856-1858.

KOSTOYANOV, A.I., MANOILOV, V.V., EFIS, YU.M. & RODIONOV, M.V. (2000): A mass-spectometer complex for measuring the isotopic composition of the difficult-to-ionize metals. *Instruments and Experimental Techniques* **43**, 91-93.

_____ & PUSHKARYOV, YU.D. (1998): Mass-spectrometric measurement of isotopic osmium content by detecting the negatively charged ions of osmium OsO_3^-. *Zavodskaya laboratoriya. Diagnostika materialov* **64**, 24-28 (in Russ.).

LEGENDRE, O. & AUGÉ, T. (1986): Mineralogy of platinum-group mineral inclusions in chromitites from different ophiolitic complexes. *In* Metallogeny of Basic and Ultrabasic Rocks (M.J. Gallagher, R.A. Ixer, C.R. Neary & H.M. Prichard, eds.). Institution of Mining and Metallurgy, London, U.K. (361-372).

MALITCH, K.N. (1999): *Platinum-Group Elements in Clinopyroxenite–Dunite Massifs of the Eastern Siberia* (*Geochemistry, Mineralogy, and Genesis*). Saint Petersburg Cartographic Factory, VSEGEI Press, St. Petersburg, Russia (in Russ.).

_____, AUGÉ, T., BADANINA, I.YU., GONCHAROV, M.M., JUNK, S.A. & PERNICKA, E. (2002a): Os-rich nuggets from Au–PGE placers of the Maimecha–Kotui Province, Russia: a multi-disciplinary study. *Mineral. Petrol.* **76**, 121-148.

_____ & BADANINA, I.YU. (1998): Natural polycomponent solid-solution series of the system Ru–Os–Ir–Pt–Fe, their genetic and applied significance. *Dokl. Earth Sci.* **363**, 1089-1092.

_____, GONCHAROV, M.M. & KOSTOYANOV, A.I. (2002b): Chemical and osmium isotope composition of PGE-mineralization from the Kunar Complex (Chelyuskin Belt, northeastern Taimyr). *In* Resources of Taimyr, Part **5** (O.N. Simonov & N.S. Malitch, eds.). VSEGEI Press, Noril'sk, Russia (144-159, in Russ.).

_____, JUNK, S.A., THALHAMMER, O.A.R., MELCHER, F., KNAUF, V.V., PERNICKA, E. & STUMPFL, E.F. (2003a). Laurite and ruarsite from podiform chromitites at Kraubath and Hochgrössen, Austria: new insights from osmium isotopes. *Can. Mineral.* **41**, 331-352.

_____, KOSTOYANOV, A.I. & MERKLE, R.K.W. (2000): Chemical composition and osmium isotopes of PGE-mineralization from the eastern Witwatersrand (South Africa). *Geology of Ore Deposits* **42**, 253-266.

_____ & LOPATIN, G.G. (1997): New data on the metallogeny of the unique Guli clinopyroxenite–dunite Massif (northern Siberia, Russia). *Geology of Ore Deposits* **39**(3), 209-218.

_____, THALHAMMER, O.A.R., KNAUF, V.V. & MELCHER, F. (2003b): Diversity of platinum-group mineral assemblages in banded and podiform chromitite from the Kraubath ultramafic massif, Austria: evidence for an ophiolitic transition zone? *Mineral. Deposita* **38**, 282-297.

MASSALSKI, T.B., ed. (1993): *Binary Alloy Phase Diagrams*. Am. Soc. Metals, Metals Park, Ohio.

MEISEL, T., WALKER, R.J., IRVING, A.J. & LORAND, J.-P. (2001): Osmium isotopic composition of mantle xenoliths: a global perspective. *Geochim. Cosmochim. Acta* **65**, 1311-1323.

MELCHER, F., GRUM, W., SIMON, G., THALHAMMER, T.V. & STUMPFL, E.F. (1997): Petrogenesis of the ophiolitic giant chromite deposits of Kempirsai, Kazakhstan: a study of solid and fluid inclusions in chromite. *J. Petrol.* **38**, 1419-1458.

MERKLE, R.K.W. & FRANKLYN, C.B. (1999): Milli-PIXE determinations of trace elements in osmium-rich platinum-group minerals from the Witwatersrand Basin, South Africa. *Nucl. Instrum. Methods Phys. Res.* **B158**, 556-561.

MINTER, W.E.L,, GOEDHART, M., KNIGHT, J. & FRIMMEL, H.E. (1993): Morphology of Witwatersrand gold grains from the Basal reef: evidence for their detrital origin. *Econ. Geol.* **88**, 237-248.

_____ & LEON, J.S. (1991): Palaeocurrent dispersal patterns of Witwatersrand gold placers. *S. Afr. Geol. Soc., Trans.* **94,** 70-85.

MOUNTAIN, B.W. & WOOD, S.A. (1988): Solubility and transport of platinum-group elements in hydrothermal solutions: thermodynamic and physical chemical constraints. *In* GeoPlatinum 87 (H.M. Prichard, P.J. Potts, J.F.W. Bowles & S.J. Cribb, eds.). Elsevier, Amsterdam, The Netherlands (57-82).

NIXON, G.T., CABRI, L.J. & LAFLAMME, J.H.G. (1990): Platinum-group element mineralization in lode and placer deposits associated with the Tulameen Alaskan-type complex, British Columbia. *Can. Mineral.* **28**, 503-535.

OBERTHÜR, T. (1983): *Metallogenetische Überlegungen zur Bildung des Carbon Leader Reef, Carletonville Goldfeld, Witwatersrand, Südafrika.* Dr rer. nat. thesis, Universität Köln, Köln, Germany.

OKRUGIN, A.V. (2002): Phase transformations and genesis of platinum-group minerals in various types of platinum-bearing deposits. *In* 9th Int. Platinum Symp. (Billings), Extended Abstr. (A.E. Boudreau, ed.). Duke University Press, Durham, North Carolina (349-353).

PALANDZHIAN, S.A., DMITRENKO, G.G. & MOCHALOV, A.G. (1994): Platinum-group element mineralization in Alpine-type ultramafites and geodynamic settings of ophiolite formation. *In* Geology and Genesis of Platinum Metal Deposits (N.P. Laverov & V.V. Distler, eds.). Nauka Press, Moscow, Russia (155-167, in Russ.).

PECK, D.C., KEAYS, R.R. & FORD, R.J. (1992): Direct crystallization of refractory platinum-group element alloys from boninitic magmas: evidence from western Tasmania. *Aust. J. Earth Sci.* **39**, 373-387.

PHILLIPS, G.N. & LAW, J.D.M. (1994): Metamorphism of the Witwatersrand gold fields: a review. *Ore Geol. Rev.* **9**, 1-31.

_____ & _____ (2000): Witwatersrand Gold Fields: geology, genesis, and exploration. *In* Gold in 2000 (S.G. Hagemann & P.E. Brown, eds.). *Rev. Econ. Geol.* **13**, 439-500.

POUJOL, M., ROBB, L.J. & RESPAUT, J.P. (1999): U–Pb and Pb–Pb isotopic studies relating to the origin of gold mineralization in the Evander Goldfield, Witwatersrand Basin, South Africa. *Precamb. Res.* **95**, 167-185.

_____, _____, _____ & ANHAEUSSER, C.R. (1996): 3.07–2.97 Ga greenstone belt formation in the northeastern Kaapvaal Craton – implications for the origin of the Witwatersrand basin. *Econ. Geol.* **91**, 1455-1461.

PRETORIUS, D.A. (1981): Gold and uranium in quartz-pebble conglomerates. *Econ. Geol., Seventy-Fifth Anniv. Vol.*, 117-138.

_____ (1991): The sources of Witwatersrand gold and uranium: a continued difference of opinion. *In* Historical Perspectives of Genetic Concepts and Case Histories of Famous Discoveries (R.W. Hutchinson & R.I. Grauch, eds.). *Econ. Geol., Monogr.* **8**, 139-163.

REIMER, T.O. (1979): Platinoids in auriferous Proterozoic conglomerates of South Africa. Evaluation of existing data. *Neues Jahrb. Mineral., Abh.* **135**, 287-314.

ROBB, L.J., DAVIS, D.W. & KAMO, S.L. (1990): U–Pb ages on single detrital zircon grains from the Witwatersrand Basin, South Africa: constraints on the age of sedimentation and on the evolution of granites adjacent to the basin. *J. Geol.* **98**, 311-328.

_____ & MEYER, F.M. (1990): The nature of the Witwatersrand hinterland: conjectures on the source area problem. *Econ. Geol.* **85**, 511-536.

_____ & _____ (1995): The Witwatersrand Basin, South Africa: geological framework and mineralization processes. *Ore Geol. Rev.* **10**, 67-94.

ROSMAN, K.J.R. & TAYLOR, P.D.P. (1998): Isotopic composition of the elements 1997. *Pure Appl. Chem.* **70**, 217-235.

ROZHKOV, I.S., KITSUL, V.I., RAZIN, L.V. & BORISHANSKAYA, S.S. (1962): *Platinum of Aldan Shield.* Academy of Sciences of the USSR Press, Moscow, Russia (in Russ.).

SHIREY, S.B. & WALKER, R.J. (1998): The Re–Os isotope system in cosmochemistry and high-temperature geochemistry. *Annu. Rev. Earth Planet. Sci.* **26**, 423-500.

SMOLIAR, M.I., WALKER, R.J. & MORGAN, J.W. (1996): Re–Os ages of group IIA, IIIA, IVA, and IVB meteorites. *Science* **271**, 1099-1102.

SOUTH AFRICAN COMMITTEE FOR STRATIGRAPHY (SACS) (1980): Lithostratigraphy of the Republic of South Africa, South West Africa/Namibia and the Republics of Bophuthatswana, Transkei and Venda (L.E. Kent, ed.). Goverment Printer, Pretoria, South Africa.

STEVENS, G., BOER, R.H. & GIBSON, R.L. (1997): Metamorphism, fluid flow and gold remobilization in the Witwatersrand Basin: towards a unifying model. *S. Afr. J. Geol.* **100**, 363-375.

STUMPFL, E.F. & TARKIAN, M. (1976): Platinum genesis: new mineralogical evidence. *Econ. Geol.* **71**, 1451-1460.

TAINTON, S. (1994): A review of the Witwatersrand Basin and trends in exploration. *In* Proc. XVth CMMI Congress (C.R. Anhaeusser, ed.). South African Institute of Mining and Metallurgy / Geological Society of South Africa, Johannesburg, **3** (Geology), 19-45.

TOMA, S.A. & MURPHY, S. (1978): Exsolution of gold from detrital platinum-group metal grains in the Witwatersrand auriferous conglomerates. *Can. Mineral.* **16**, 641-650.

TUTTAS, D. (1992): The measurement of osmium isotope ratios using negative thermal ionization. *Application News* **1**, 1-20.

TWEEDIE, E.B. (1986): The Evander Goldfield. *In* Mineral Deposits of Southern Africa **1** (C.R. Anhaeusser & S. Maske, eds). Geological Society of South Africa, Johannesburg, South Africa (705-730).

VENNEMAN, T.W., KESLER, S.E., FREDERICKSON, G.C., MINTER, W.E.L. & HEINE, R.R. (1996): Oxygen isotope sedimentology of gold- and uranium-bearing Witwatersrand and Huronian Supergroup quartz-pebble conglomerates. *Econ. Geol.* **91**, 322-342.

WAGNER, P.A. (1973): *The Platinum Deposits and Mines of South Africa*. C. Struik (Pty) Ltd., Cape Town, South Africa.

YIN, Q., JAGOUTZ, E., PALME, H. & WANKE, H. (1996): NUR – a possible proxy for CHUR reference for Re–Os system derived from $^{187}Os/^{188}Os$ ratio of the Allende CAI. *Lunar & Planetary Sci Conf.* **XXVII**, 1475-1476 (abstr.).

YOUNG, R.B. (1907): Notes on the auriferous conglomerates of the Witwatersrand. *Trans. Geol. Soc. S. Afr.* **10**, 17-30.

Received July 18, 2003, revised manuscript accepted November 24, 2003.